AFOSR SCIENTIFIC REPORT
AFOSR TR 72-0322

ASRL TR 162-2

LOW CYCLE COMPRESSIVE FATIGUE FAILURE OF E GLASS-EPOXY COMPOSITES

Gerald Sedor
Rodney K. Watterson

MASSACHUSETTS INSTITUTE OF TECHNOLOGY

AEROELASTIC AND STRUCTURES RESEARCH LABORATORY

March 1972

AIR FORCE OFFICE OF SCIENTIFIC RESEARCH

UNITED STATES AIR FORCE

CONTRACT NO. F44620-70-C-0020

APPROVED FOR PUBLIC RELEASE; DISTRIBUTION UNLIMITED

1

56

UNCLASSIFIED

Security Classification

DOCUMENT CONTROL DATA - R & D

(Security classification of title, body of abstract and indexing annotation must be entered when the overall report is classified)

1. ORIGINATING ACTIVITY (Corporate author) MASSACHUSETTS INSTITUTE OF TECHNOLOGY DEPT OF AERONAUTICS AND ASTRONAUTICS CAMBRIDGE, MASSACHUSETTS 02139	2a. REPORT SECURITY CLASSIFICATION UNCLASSIFIED 2b. GROUP

3. REPORT TITLE

LOW CYCLE COMPRESSIVE FATIGUE FAILURE OF E GLASS-EPOXY COMPOSITES

4. DESCRIPTIVE NOTES (Type of report and inclusive dates)

Scientific Interim

5. AUTHOR(S) (First name, middle initial, last name)

GERALD SEDOR RODNEY K WATTERSON

6. REPORT DATE March 1972		7a. TOTAL NO. OF PAGES 56	7b. NO. OF REFS 26
8a. CONTRACT OR GRANT NO	F44620-70-C-0020	9a. ORIGINATOR'S REPORT NUMBER(S) ASRL TR 162-2	
b. PROJECT NO.	9782-02		
c.	61102F	9b. OTHER REPORT NO(S) (Any other numbers that may be assigned this report) AFOSR-TR-72-0322	
d.	681307		

10. DISTRIBUTION STATEMENT

Approved for public release; distribution unlimited.

11. SUPPLEMENTARY NOTES TECH, OTHER	12. SPONSORING MILITARY ACTIVITY AF Office of Scientific Research (NAM) 1400 Wilson Boulevard Arlington, Virginia 22209

13. ABSTRACT

Low-cycle fatigue tests with a mean compressive stress were conducted on modified "dogbone" type specimens of 0° -90° 3M SCOTCHPLY laminates with fiber volume fractions ranging from 45 to 60 percent. The test results indicate that compressive fatigue strength decreases as a linear function of log(cycles), and that strain increases linearly up to approximately 60 percent of fatigue life. Beyond this point a significant increase in strain is observed, indicating that accumulation of major damage is concentrated in the last 40 percent of fatigue life. The progress of damage during fatigue was investigated independently by optical microscopy. These observations indicate that the predominant damage effect is debonding of 0° fibers (parallel to the load axis), followed by fracture of groups of adjacent fibers. Inter-ply delamination is also observed in some cases. Based on the test results and microscope observations, the failure mechanism of progressive debonding leading to local buckling and fracture of the 0° fibers is proposed. The final result is an inclined shear fracture when cracks in the damaged axial plies propagate through the transverse plies. The effects of misaligning a small percentage of the axial plies within the laminate, and of a 21-day immersion in sea water were also studied. Compressive fatigue strength is found to decrease due to both of these effects.

DD FORM 1 NOV 68 1473

UNCLASSIFIED

Security Classification

14 KEY WORDS	LINK A		LINK B		LINK C	
	ROLE	WT	ROLE	WT	ROLE	WT
COMPRESSIVE FATIGUE FAILURE						
FATIGUE OF COMPOSITES						
E-GLASS EPOXY FATIGUE						

Acknowledgements

The authors wish to express their appreciation to Professor James W. Mar and Dr. O. Orringer of the M.I.T. Department of Aeronautics and Astronautics and to Dr. Lawrence A. Shepard of the U. S. Army Mechanics and Materials Research Center for their constant encouragement and guidance. Frequent advice and extensive reference materials were provided by Professor F. J. McGarry and Mr. Richard Dauksys of the Civil Engineering Department. Mr. Oscar Wallin of ASRL and Mr. Arthur Rudolph of the Civil Engineering Department assisted in the cutting and machining of the test specimens. Instruction and advice in polishing and photomicroscopy technique was provided by Mr. Guenther Arndt of the Metallurgy Department. The report manuscript was typed by Miss Frances Moy. The work described in this report was supported by the U. S. Air Force Office of Scientific Research under contract number F44620-70-C-0020.

TABLE OF CONTENTS

SYMBOLS

E - Young's modulus
γ - Volume fraction
N - Number of loading cycles
ν - Poisson's ratio
ρ - Specific gravity
S - Maximum stress in cyclic loading
σ - Stress
ω - Weight fraction

SUBSCRIPTS

c - Composite
d - Debonding
f - Fiber
G - Glass fiber
m - Matrix
R - Resin (matrix)
V - Voids

I. INTRODUCTION

Recent emphasis on the development of deep-diving submersibles for scientific, commercial and military purposes has indicated the need for development of high-strength structural materials. Particular attention is being focussed on glass reinforced plastic composites by the United States Navy [15, 17, 18, 19, 22]. The primary interest in these materials lies in their high strength-to-weight ratios, which permit the construction of hulls with acceptably low weight-to-displacement ratios and consequently, with high payload capabilities. For example, filament wound glass reinforced plastic laminates have been produced with static compressive strengths of 170,000 psi and higher, proving strength/weight ratios exceeding 2×10^6 inches. In comparison, high-strength steels (e.g., HY-140) have a strength/weight ratio of 0.5×10^6 inches, while high-strength titanium alloys (e.g., HY-120) have a ratio of 0.8×10^6 inches [14].

The ultimate applicability of glass reinforced plastic composites to the construction of deep submersible hulls will depend upon material reliability in an operational environment. Perhaps the most significant factor in this application is the high stress, low cycle fatigue environment associated with repeated excursions of a submersible vehicle to its maximum operating depth. In this regard, Broutman and Krock state that "...the one type of behavior which appears more critical than the others and, indeed, may be a current limitation of the material, is its response to cyclic loads, or its fatigue life." [7] This report reviews the literature available on the subject of compressive and fatigue behavior of composites and summarizes the research results obtained by the present authors [25, 26].

Experimental observations of fatigue behavior in composites have generally been concentrated on tests in which the mean stress has been either tensile or zero. Boller [2, 3, 4, 5, 6] has made an extensive fatigue study of 3M "Scotchply", using both E and S glass filaments, under zero mean stress. Boller's studies are primarily collections and displays of data with little effort made to explain the mechanism of failure. After evaluating many speci-

men configurations, the present authors chose a shortened version of Boller's test specimen for their research.

Broutman and Sahu [8] have investigated the tensile fatigue of Scotchply in a cross-ply layup. They report that the residual tensile strength of laminates subjected to fluctuating tension with a maximum stress decreases as the number of cycles increases. Also, they suggest a failure mechanism for tensile fatigue. Having observed that cracks appear in plies with fibers perpendicular to the load axis during the first cycle (if the stress is above 20 per cent of UTS), and that cracks appear in plies with fibers parallel to the load axis only when the stress level exceeds 75 per cent of UTS, Broutman and Sahu conclude that the failure mechanism involves propagation of the cross ply cracks into the in-line plies, accompanied by delamination as the cracking progresses. The initial quickly formed cracks are thought to be caused by high stress concentration in the resin between those fibers oriented at 90° to the load axis.

Fried [13] has investigated the response of cross-ply filament wound composites to static compressive stress. He found that failure in compression tends to occur by a debonding process at the interfaces between perpendicular plies, in a mode which is similar to the failure mechanism in shear. In general, voids appear to control the failure process, and an inverse relationship was found between shear or compressive strength versus void content. As a consequence, a direct linear relationship between compressive and shear strength was found to exist. Fried also noted that failure is catastropic in the immediate area of the break, with considerable glass filament fracture. However, in areas somewhat removed from the break, sharp interface separations were observed. This separation or debonding was found to be remarkably similar to that observed in interlaminar shear tests of cross-ply laminates. Fried concludes that compressive failure with any void content in excess of 1 per cent is a debonding process and suggests that compressive failure due to resin yield is a limiting value which can be attained theoretically, but not exceeded.

With regard to compressive fatigue behavior, Fried et. al. [14] report that water immersion of filament wound composites resulted in a definite reduction in fatigue strength at stress levels below 80 per cent of ultimate. Freund and Silvergleit [12] have surveyed the data collected in four years of compressive fatigue tests and concluded that a "percentage of ultimate" concept exists, wherein the applied fatigue stress, as a percentage of true ultimate static stress, can be used to predict reliably the life of glass reinforced plastic materials. This percentile of true static stress appears to be a constant for any given number of cycles, irrespective of the test method, specimen fabrication or specimen geometry. The weak points in this study are that a large amount of scatter exists in the surveyed fatigue data, and that the ultimate static strength chosen as a reference for each test was at best a matter of judgment. Finally, Cole et. al. [10] have investigated damage under biaxial compressive fatigue loading using ultrasonic techniques.

Based on the above literature survey, the present authors set up a research program to investigate the behavior of 3M Scotchply under high stress, low cycle compressive fatigue. When reliable S-logN data had been obtained, specimens were loaded for some number of cycles less than failure, sectioned, and analyzed for damage progress. Also, some brief tests were conducted on specimens having a small percentage of the in-line plies misaligned, and on specimens which had been subjected to a sea water immersion.

II. PROCEDURE

Laminate Fabrication

The material chosen for this research program was 3M Scotchply 1002, a preimpregnated resin reinforced with unidirectional unwoven E glass fibers. The following fabrication technique was adopted after experiments with several others:

1. Using Scotchply tape, 12 inch square laminates were laid up to desired thickness. A 30 layer laminate was generally used. The layers were of a cross-ply configuration with adjacent layers having their fibers perpendicular. (See Table 1 in Appendix A.)
2. The laminate was wrapped in an envelope containing a releasing agent so that it could be removed after the application of heat and pressure during the curing procedure.
   a. As indicated in Appendix A, some laminates were wrapped in a silicon paper, S.C.W. 33, provided by 3M specifically for this purpose.
   b. The remaining laminates were wrapped in a mylar envelope sprayed with "Frekote 33", a United Chemical product. This releasing agent proved superior to the silicon paper.
3. The following cure cycle was used on a hydraulic press with thermostatically controlled platens:
   a. The platens were heated to 350°F and the laminates rested on the platens for five minutes.
   b. The platens were closed to contact pressure and the pressure was gradually increased to 30 psi over a five minute period.
   c. The pressure and temperature were maintained at 30 psi and 350°F for 10 minutes.
   d. The laminate was cooled at atmospheric pressure to room temperature.

This cure, with no post cure heat treatment, is advertised by 3M to produce room temperature mechanical properties of about 85 percent of those available with a 16 hour post cure at 280°F.

Specimen Shape and Preparation

The specimen geometry shown in Figure 1 was chosen after experimentation with various other sizes and shapes found in the literature. It is based on the fatigue specimens used by Boller in his fatigue studies [2, 3], modified in length and width to

eliminate the end sections which are fitted into a clamp for tensile testing. Since this study was to be limited to compressive stresses, it was determined that clamping of the ends would not be required and a shorter specimen would more closely approach the relative dimensions of the compressive specimen described in the ASTM Test Methods [1].

The fatigue specimens used by Broutman and Sahu in their study [8], although similar to that used by Boller, provided for a gage section of constant width and two inches in length. This shape was rejected in favor of Boller's shape, based on the desire to conduct a microscopic analysis of specimens which had been fatigued to less than failure. The varying cross-section area of the selected shape was considered advantageous in locating more precisely the section most likely to suffer fatigue damage, and consequently of more interest in subsequent microscopic analyses.

To prepare the specimens in the desired shape, the 12-inch square laminate was first cut into rectangular shapes of approximately the desired dimensions with a circular diamond abrasive wheel. Care was taken to ensure that all cuts were made along the axis of either the zero degree plies or the ninety degree plies. A Tensil-Kut machine was then used to obtain the required rectangular dimensions. Particular care was taken to ensure that the edges to be loaded were smooth, flat, and parallel, as specified in the ASTM Test Methods for compressive testing [1]. The specimens were then machined to provide for the desired radius of curvature, with a one-quarter inch width at the minimum section.

Fatigue Testing

The testing machine used for compressive and fatigue testing was a Baldwin SR-4 Compression and Tension Testing Machine, with test load readout and automatic cycling capability, in which upper and lower load limits can be set. To eliminate the effects of any misalignment of the specimen in the machine, a ball-joint surface was installed in the upper cross-head.

A support jig was used to prevent buckling of the specimens under compression. The support jig design was based on that shown in Figure 4 of Reference [1], modified to suit the dimensions of the specimen.

A dial gage extensometer was attached to the upper crosshead for indication of specimen strain under load. The use of strain gages was precluded by the installation of the support jig. However, since strain data was not essential to the primary purpose of the study, the dial gage installation was considered entirely adequate.

The basic test objective was to establish the ultimate compressive strength and the compressive fatigue S-logN curve for each laminate. Progressive damage within the material could then be investigated by cycling the specimens at a percentage of UCS and stopping at various stages of fatigue life before failure. The stress level selected was 75 $\pm$ 5% of UCS. The number of cycles to which a particular specimen was cycled was chosen arbitrarily, with strain data providing some indication of proximity to failure.

The calculated load for the particular stress desired could be pre-set into the machine to within approximately 15% of the desired value. The maximum load setting was generally refined within the second or third cycle to approach more closely the desired level. The lower limit for all fatigue cycling was set at approximately 1 to 3 per cent of ultimate. The cycling rate for all tests was set at approximately 6 cycles per minute. This cycling rate was also used for the half-cycle tests for ultimate compressive strength.

Tape Misalignment and Environmental Tests

Laminates 9, 12 and 13 were fabricated with some of the plies misaligned by 15, 30 or 45 degrees. (See Table 1 of Appendix A for details.)

To investigate the effects of sea water immersion on the laminate, specimens from Laminate 11 were fully prepared, weighed, and completely immersed in a glass jar containing sea water

obtained from the Nahant Beach area. To achieve the most severe effects of immersion, specimens were immersed with all cut edges exposed to the sea water. The immersed specimens were maintained at atmospheric pressure and room temperature throughout the entire immersion period of 21 days.

Upon completion of the immersion period, the specimens were immediately weighed and fatigue tested. Selected specimens were then sectioned for microscopic analysis.

Measurement of Void Content

Void content of each laminate was determined by resin burnout and wet weighing techniques. The characterization formulas described by Cole, et. al., [10] were used and are listed below.

$$\text{Composite Specific Gravity } (\rho_c) = \frac{\text{Weight in Air}}{\text{Weight in Air - Weight in Water}}$$

$$\text{Resin Volume \%} = \left[\frac{\text{Resin Weight \%}}{\text{Resin Specific Gravity}}\right] \cdot \left[\text{Composite Specific Gravity}\right]$$

or,
$$\gamma_R' = \frac{\omega_R}{\rho_R}\rho_c$$

Similarly, Glass Volume % = $\gamma_G' = \frac{\omega_G}{\rho_G}\rho_c$

Void Volume % = 100 - (Resin Volume % + Glass Volume %)

or,
$$\gamma_V' = 100 - \gamma_R' - \gamma_G'$$

Glass fiber weight was determined by burning off the resin at 630°C and weighing the residue. In order to achieve accurate results, two parameters must be known accurately, the specific gravity of the resin and the specific gravity of the glass fibers. The typical specific gravity of an E-glass fiber is given by Broutman and Krock [7] as 2.54 $\pm$ .03. However, as shown by Otto [23], the density of E-glass is increased by heat treating, due to the compaction of glass at elevated temperatures. This density change remains when the glass is cooled to room temperature. The resin burnout technique used to determine void content, then,

changes one of the "constants" used in subsequent calculations. Using Otto's results, a value of 2.59 was estimated for the specific gravity of the glass fibers after burnout.

The resin specific gravity is also subject to some question. The specific gravity of Type 1002 resin is listed in one 3M Company Memorandum as 1.16, with the qualifying remarks that the properties of the resin casting for which the data is given would not necessarily be equal to the properties of the resin portion of a glass reinforced laminate molded under pressure with the resin in thin layers around and between fibers [21]. Other 3M Company technical data [20] indicates that a composite specific gravity of 1.84 is achieved with a resin content of 36% by weight. Using this information with the assumed fiber specific gravity of 2.59, the resin specific gravity was calculated to be 1.26. This latter figure is used in all void content calculations.

Since the assumed values of resin and fiber specific gravity were somewhat questionable, a separate void content determination was conducted by the systematic point count method recommended by DeHoff and Rhines [11] and Hilliard and Cahn [16].

To conduct the point count, a two inch square grid was constructed on a clear plastic sheet. Ten grid lines were drawn in each direction, resulting in 100 grid corners. The size of the grid and the number of corners were based on optimum considerations outlined by Hilliard and Cahn, with the assumption that void content was approximately 3%.

To calculate void content, the grid was placed over randomly selected sections of the photomicrographs of the reference specimens. The total fraction of grid corners falling on void spaces then provided an unbiased estimate of the void volume fraction.

Microscopic Analysis

The following definitions are used to refer to sectioned faces of the sample with respect to the coordinate system shown in Figure 2:

1. Perpendicular Face - Face in XY plane, showing ends of fibers in line with the load and lengths of fibers perpendicular to the load.
2. Parallel Face - Face in XZ plane, showing ends of fibers perpendicular to the load and lengths of fibers in line with the load.
3. In Line Face - Face in YZ plane, showing lengths of fibers in line with and perpendicular to the load.

Sectioned samples were mounted in Quickmount and polished with paper down to 10 microns. A low speed electric polishing wheel with diamond paste was used to 1 micron and a Syntron polisher with aluminum oxide powder was used to .3 microns to avoid matrix damage during polishing.

Microscopic analysis and photography was done on a Reichert optical metallograph using a Nomarski interferometer attachment to bring out the fiber detail.

III. EXPERIMENTAL RESULTS

General Observations

On a macroscopic level, failures under compressive static or fatigue loading tended to occur in a shear mode when the specimens were restrained from buckling by using the support jig. The shear line generally occurred near, but not precisely centered on the section of minimum area. Three basic variations in shear failure were observed:

(1) A slant fracture along a single fracture plane inclined approximately 45 degrees to the load axis.

(2) A double slant fracture, or single "V", with either side of the V inclined at approximately 45 to 60 degrees to the load axis, and extending throughout the thickness of the specimen.

(3) A double "V", usually extending through only part of the thickness.

Typical examples of the above variations in shear failure are illustrated in Figure 3. A fourth type of failure, not shown,

occurred when the support jig was not used. In this case, failure occurred by delamination and buckling of individual plies, usually starting at the outer surface plies and progressing inward toward the center of the specimen.

Failures were generally accompanied by a very sharp cracking noise with a simultaneous rapid decrease in load indication. In some of the fatigue tests, a very slight cracking noise was heard prior to ultimate failure. This noise was generally not accompanied by any significant decrease in load indication. However, the indicated strain generally showed a rapid increase during subsequent cycling up to the point of failure. The actual failure point was defined as that point at which a rapid decrease in applied load indication was observed, and in all cases was accompanied by a characteristic cracking noise.

Another macroscopic phenomenon observed was the formation of transverse lines and very fine cracks in outer surface plies with fibers oriented at 90 degrees to the load axis. The observed lines were parallel to each other and normal to the load axis, and extended over the entire width of the specimen. In some failed specimens, the shear fracture appeared to originate from cracks of this type, but no consistency was observed in this regard. The transverse lines and cracks were observed in fatigued specimens, in which cycling was stopped prior to failure, as well as in failed specimens.

In an attempt to determine the effect of this transverse cracking on the fatigue strength of the laminate, the 90 degree surface ply was removed from several specimens by light sanding. Although this eliminated the transverse lines, no significant effect on laminate strength was noted.

A summary of the measured specimen properties and ultimate strength data will be found in Appendix B.

Mechanical Behavior

The results of fatigue testing of a material are generally presented in the form of a curve showing maximum applied stress

S versus the logarithm of the number of cycles to failure N. S-logN data for Laminates 6, 10, and 11 are plotted in Figures 4, 5, and 6 respectively. The results for all three laminates are combined in Figure 7 by normalizing fatigue stress to a percentage of ultimate compressive stress.

Figure 8 shows the results of tests of specimens with misaligned fibers compared to Laminate 6. Laminates 9-15, 9-30, and 9-45 with 4 plies misaligned at 15°, 30°, and 45° respectively were compared to Laminate 6 because it best approximated the void volume percentages of 9-15, 9-30, and 9-45. Also, similar fabrication methods were used for these laminates. Laminate 9-15 supports a maximum stress of about 93 percent of the reference for an equivalent number of cycles. There is no appreciable difference between the strength reduction for the 30° misaligned plies and the 45° misaligned plies; both support a maximum stress of about 72 percent of the reference for an equivalent number of cycles. The comparisons for reduction in fatigue strength are based on the relative performance of the laminates at 30 cycles.

Figure 9 shows the results of tests of additional specimens with misaligned fibers compared to Laminate 11. Laminates 12-30 and 13-15 with four plies misaligned at 30° and 15° respectively were compared to Laminate 11 for the reasons mentioned above. Laminate 13-15 supports a maximum stress of about 92 percent of the reference for an equivalent number of cycles and Laminate 12-30 supports a maximum stress of about 76 percent for an equivalent number of cycles. Again the comparisons for reduction in fatigue strength are based on the relative performance of the laminates at 30 cycles.

The results of testing Laminate 11 before and after sea water immersion are compared in Figure 10. Immersion in sea water for 21 days resulted in an average water absorption of 0.226% by weight. Compressive fatigue strength for the immersed specimens showed a decrease of approximately 6 to 10 percent throughout the range tested, as shown in Figure 10.

In reviewing the S-logN curves, it should be noted that the ultimate compressive stress for each laminate was arbitrarily defined as the highest compressive stress sustained by any of the specimens of that laminate prior to failure. In addition, it should be noted that all curves were arbitrarily started at one cycle. Those failures indicated on the curves as occurring on the first cycle could more accurately be shown as occurring at the first half-cycle, when the peak compressive load is applied.

An examination of the S-logN curves indicates that, within the range tested, fatigue strength decreases in an approximately linear manner with an increase in log (cycles). Laminates 10 and 11 exhibited comparable fatigue strengths, with Laminate 11 having a slightly higher ultimate compressive strength. Laminate 6, while exhibiting an S-logN slope similar to the other laminates, had a fatigue strength approximately 20% less than Laminates 10 and 11 throughout the range tested.

The strain history of the selected specimens, shown in Figure 11, indicates that the strain at maximum stress increases in an almost linear manner up to approximately 60% of the fatigue life of the material. Beyond this point, there is a marked increase in the rate of permanent strain accumulation. A summary of data for fatigue tests can be found in the tables of Appendix B.

Microscopic Analysis

Sections of selected specimens at various stages of fatigue life were examined in order to investigate progressive damage of the material under compressive fatigue loading. Figures 12 through 23 are photomicrographs of some of the reference specimens. Figures 24 through 28 illustrate the behavior of specimens with misaligned plies. Figures 29 through 31 represent specimens which were immersed in sea water prior to testing.

Figures 12 through 23 support the following observations concerning compressive fatigue failure in cross-ply laminates.

1. The original internal damage occurs in the plies in line with the load. The damage appears as a separation within the plies and spreading of the fibers. This damage is best shown on the parallel face. (See Figure 2 for definition of faces.)

2. The damage discussed above removes the lateral support for the fibers and results in a local buckling failure of the fibers in line with the load.
3. The failure progresses through the thickness tending to debond the plies with in-line fibers from the cross-plies. This damage is shown best on the perpendicular face.
4. Transverse surface cracks appear early in the outer layer containing plies with fibers perpendicular to the load. (Note that with an even number of layers one surface layer always has fibers perpendicular to the load direction.)

The following guide is included to aid in interpreting Figures 12 through 23.

Figure	Above Items Supported	Laminate	Face	Remarks
12, 13, 14	1	11	Parallel	Note the progressive separation in the plies in line with the load as one progresses from a nontested specimen through two stages of compressive fatigue testing.
15, 16	3	11	Perpendicular	Note the separation of in line and cross-plies as failure progresses.
17, 18	1	10	Parallel	These figures show the same progressive separation damage in Laminate 10 as seen in Figures 12, 13, and 14 for Laminate 11.
19	3	10	Perpendicular	This figure shows the same separation of in line and cross-plies in Laminate 10 as seen in Figure 16 for Laminate 11.

Figure	Above Items Supported	Laminate	Face	Remarks
20		6	Parallel	Compare the excessive void content in Laminate 6 to the smaller void content in Laminates 11 and 10 shown in Figures 1[illegible] and 17 respectively.
21		11	Parallel	This photograph shows the normal appearance of the sectioned specimen after extensive cycling. There is generally little damage visible. The damage shown in Figures 12, 13, and 14 is generally not extensive.
22	4	11	In Line	This figure shows the transverse surface crack discussed above.
23	1, 2, 3	11	Parallel	This figure shows a failure. Note the sheared fibers and the separation of the in line and cross-plies at the left of the picture.

Figures 24 through 28 support the following observations concerning compressive fatigue failure in cross-ply laminates with misaligned plies.

1. The failure originates in the misaligned plies.
2. The major damage centers in the area of the misaligned fibers.
3. Delamination is prevalent in the misaligned fibers.

The following guide is included to aid in interpreting Figures 24 through 28.

Figure	Above Items Supported	Laminate	Face	Remarks
24, 25	2	12-30	Parallel	The failure is exaggerated in the misaligned fibers.
26	3	12-30	Perpendicular	A separation occurs between the misaligned fibers and adjacent fibers in many cases. This damage was also noticeable within the misaligned plies.
27	1	9-45	45° plane	The fiber lengths shown are the plies misaligned by 45°. These fibers have failed with little other damage noticeable outside the misaligned plies.
28	2, 3	13-15 12-30		The major damage occurs in the area of the misaligned fibers. The failure travels lengthwise along the misaligned fibers or the interface between the misaligned fibers and aligned fibers.

Comparison of Figures 29 through 31 with Figures 12 through 23 indicates that the same basic damage mechanisms operated in the immersed specimens as those which operated in the reference specimens. Also, there is apparently no significant void growth caused by immersion.

IV. DISCUSSION

Laminate Static Strength

Scotchply 1002 is advertised by 3M Company as having a compressive strength of 75,000 psi in the cross-ply configuration with the load applied in one of the fiber directions. However,

the expected strength is 85 percent of 75,000 psi or 63,750 psi without post curing. Compare the reference laminates' fiber content and average ultimate compressive strength to that advertised by 3M:

Laminate	Fiber Weight Percentage	Void Volume Percentage*	Average Ultimate Compressive Strength (Average 1/2 Cycle Failures)
Advertised	64	Not Given	63,750 psi
6	66.5	6.55 (8.50)	65,500 psi
10	75.6	2.4 (5.33)	77,700 psi
11	77.4	2.25 (4.67)	77,100 psi

The higher fiber content and lower void content explain the higher strength of laminates 10 and 11.

Void Areas

The dark areas identified as voids on the microscopic photographs were originally suspected of possibly being dirt or polishing compound. However, numerous efforts at cleaning with a solvent and an ultrasonic cleaner and, in some cases repolishing, failed to remove or change the appearance of these areas. The reduction in void content in Laminates 10 and 11 over that of Laminate 6 is attributed to more careful assembly techniques. The relatively high void content found in all laminates is attributed to the use of a relatively low molding pressure (30 psi), as well as the absence of vacuum bag molding techniques. In the determination of void content, the systematic point count method, while producing significantly higher results, confirmed in a qualitative manner the results of the resin burnout method. The higher results of the point count method may be attributed to the difficulty encountered in the visual identification of voids.

The average water absorption of 0.226% by weight over the 21-day immersion period is slightly higher than would be predicted using the manufacturer's data in Appendix A, but is in general

*Void content figures in parentheses were calculated by the point count method. The other figures were obtained by the resin burnout method.

agreement with the results of Fried, et. al., [14] for a high void content material under atmospheric pressure.

Mechanical Behavior

The linear characteristic of the S-logN curves in the low cycle range tested, and the absence of an endurance limit, are in agreement with the results of similar work found in the literature. Relatively little decrease in fatigue strength occurs in specimens with plies misaligned by 15 degrees, while there exists a significant decrease when the misaligned plies are at 30 or 45 degrees to the load axis. This leads to the conclusion that an unintentional small misalignment during manufacture will have only a small adverse effect on the compressive fatigue strength of the laminate. Fried's conclusion that "wet" and "dry" fatigue data could be clearly defined only at lower stress levels [14] was not supported by this study. As shown in Figure 24, the reduction in fatigue strength due to water immersion is more pronounced at the higher stress levels.

The strain history data, plotted for selected specimens in Figure 11 proved to be of value as an indicator of proximity to fatigue failure. The characteristic knee in the curves at approximately 60% of fatigue life is consistent in all specimens tested. It is interesting to note that for Specimen 6X, for which the cycling was stopped prior to failure, the calculated fatigue life based on the knee occurring at the 60% point is in excellent agreement with the S-logN curve for this laminate. It is apparent from the form of the strain history curves that two processes occur in the laminate. The relatively minor increase in strain from 0 to 60 percent of specimen life characterizes a mechanical modulus softening effect, perhaps accompanied by limited void growth and other minor damage. At 60 percent of life, the permanent strain accumulation rate increases significantly, indicating that major damage is now being done.

Microscopic Observations

Approximately 50 specimens were sectioned and examined. The predominant effect observed was damage within the plies oriented parallel to the load axis. This damage is characterized by axial debonding of fibers, fracture of groups of adjacent fibers, and total absence of fiber and matrix in elongated regions several hundred fiber diameters in length. Although many specimens exhibited interlaminar separations, damage within the axial plies was observed the most frequently. Figures 13, 14, 18, 30(b) and 31(b) show typical examples of this type of axial damage, while interlaminar separation may be seen in Figures 16, 19 and 31(a). The axial damage was consistently within, rather than at the interlaminar surfaces of the axial plies.

The existence of specimen damage is indicated by the above mentioned non-uniform, elongated dark areas in the photomicrographs. It is assumed that the damaged fibers and matrix in these areas were removed during the polishing process, leaving a void-like space. Actual voids, resulting from the fabrication process, while varying considerably in size from one laminate to another, are generally characterized by somewhat irregular but rounded boundaries. This can be observed in the relatively small voids appearing in Laminate 11 (Figure 12) and the large voids of Laminate 6 (Figure 20).

Failure Mechanism Hypothesis

In developing a probable failure mechanism, one must first consider the observed tendency of fatigue damage to occur most frequently within the axial plies. A simplified column analogy may be applied to the entire axial ply located between two transverse plies, as well as to the individual axial fibers within the axial ply. Progressive failure of individual axial fibers by local buckling, most likely in the shear or "in phase" mode [24] may then lead to a shear type failure of the axial ply which results in transmission of cracks through the adjacent transverse plies until fracture occurs.

The individual axial fiber may be considered to be supported along its length and restrained from buckling by the adjacent matrix material. In an analogous manner, the entire axial ply may be considered to be supported by and restrained from buckling through its bonding to adjacent transverse plies. Hence, a debonding mechanism must be proposed for the initial stages of fatigue damage.

Debonding between individual axial fibers and the adjacent matrix is the most probable mechanism. The compressive axial load on a specimen causes a transverse expansion due to the Poisson effect. Since the Poisson's ratio of the epoxy matrix is greater than that of the glass fibers, the matrix expands transversely more than the glass, tending to create an interfacial tensile debonding stress. Broutman and Krock [7] give the following expression for debonding stress, in terms of fiber and matrix properties:

$$\sigma_d = -\epsilon \left[\frac{(\nu_m - \nu_f) E_f E_m}{(1+\nu_m) E_f + (1-\nu_f - 2\nu_f^2) E_m} \right]$$

where ε is the applied axial strain, E refers to Young's modulus, ν refers to Poisson's ratio, and the subscripts f, m refer to fiber and matrix, respectively.

In the specimens tested, the transverse expansion was most apparent near the center section. For those specimens cycled to failure, the area immediately adjacent to the failure appeared to experience the greatest expansion. The amount of expansion could be qualitatively estimated from the impressions imparted to the specimens by the contact surfaces of the support jig.

Debonding between adjacent plies, more properly termed delamination, was observed to be the failure mechanism whenever the support jig was not used. The use of the support jig restricts the lateral expansion and delamination tendency. The adjacent transverse plies, then, act to support the axial "ply column"

and prevent buckling of the axial ply.

The observed cases of delamination, similar to those shown in Figures 16 and 19, could be explained by the tendency of elongated voids to appear in this interlaminar area. This hypothesis is supported by the findings of Fried [13], who concluded that such voids decrease the total bonded area and may act as loci for initiating the debonding, hence they constitute the primary factor in determining compressive strength.

The strain measurements taken during the fatigue tests add additional insight into the failure process. As indicated in Figure 11, the strain rate appears to be constant with increasing cycles up to approximately 60% of fatigue life. A significant increase in strain rate is found beyond this point. It is proposed that during the first 60% of fatigue life the only significant damage occurring is that of circumferential debonding between individual fibers and matrix within axially aligned plies. This is borne out by Figure 21 in which Specimen 11BK is shown after cycling to somewhat less than 50% of expected fatigue life. No damage is apparent within the plies or at the interlaminar surface.

At the 60% point, it is proposed that axial fiber debonding has progressed to such an extent that the lateral support offered by the matrix has degraded enough to permit significant local fiber buckling damage. This damage probably initiates within the axial plies at regions of higher void concentrations. Local fiber buckling, with its resultant higher strain accumulation rate, continues until the damage within the axial plies results in cracks which are eventually transmitted through the transverse plies at fracture.

The above failure mechanism is consistent with the results obtained from the misaligned ply tests. The four adjacent layers of misaligned plies give a large thickness without the lateral support of the crossplies. Consequently, one would expect the separation effects to be large in the misaligned plies. Also less resin support would have to be removed from the fibers in these

plies in order to cause buckling and failure of the composite. Figure 27 supports this hypothesis.

Figure 28 also supports the idea of failure originating in the misaligned plies. Specimen 12-30-C in particular shows both surfaces expanded, indicating that the failure progressed outward from the interior of the composite. Specimen 13-15-A is the only one of the four specimens in Figure 28 which suggests that failure did not initiate in the misaligned ply region. Considering the unpredictability of the initial void content and distribution, such a result is possible if the in line plies had a much higher initial void content than the misaligned plies. The failure appearance of Specimen 13-15-A was an exception rather than the rule.

It is further proposed that the failure mechanism described above is identical in the specimens subject to sea water immersion. The finding that immersion reduced fatigue strength could be attributed to the effect of adsorbed moisture on the E-glass fibers. Broutman and Krock [7] state that, although the precise effect is still not known after years of experimentation, general agreement exists that moisture will decrease the strength of glass fibers.

The void content of Laminate 11 was seen to have increased somewhat by the water immersion. It is proposed that the absorbed water is concentrated within existing voids, and tends to degrade these voids by its corrosive effect. Hence, the effect of existing voids on the compressive strength of the laminate is further emphasized by the absorption of water into these voids.

Comparison with Other Studies

Broutman demonstrated the existence of circumferential interface separation or debonding with the electron microscope. He further pointed out that for densely packed fibers the triangular shaped matrix section between fibers becomes a highly stressed area and is subject to failure by crack propogation [9]. Broutman and Sahu found a systematic crack growth in the perpendicular and

parallel faces as tensile fatigue progressed [8]. Compressive fatigue does not produce similar sharply defined cracks.

Fried credits compression failure in a similar material to a debonding process at the interface between perpendicular plies [13]. The process he describes appears to accompany but not initiate failure in compressive fatigue. Fried also noted that in the immediate area of the break, failure is catastropic, with considerable glass filament breakage. However, in areas somewhat removed from the break, a sharp separation at an interface between adjacent plies was observed. This general observation is true also for compressive fatigue. Figure 23 shows the catastropic failure with considerable glass filament breakage and Figures 16 and 19 show the separation at a distance somewhat removed from the break.

Freund and Silvergleit [12] concluded that a percentage of ultimate concept exists in compressive fatigue of similar materials wherein the applied fatigue stress, as a percentage of true ultimate static stress, can be used in reliably predicting the fatigue life of glass reinforced plastic material. They also indicated that the S-logN curve for glass reinforced plastic is linear for a fatigue stress above 60 percent of ultimate uniaxial compressive stress. Figure 7 supports these conclusions.

V. CONCLUSIONS

On the basis of the investigations reported here [25, 26] the following conclusions may be drawn about the mechanical behavior of glass fiber-epoxy matrix composite laminates in compressive fatigue:

1. Failure is initiated by debonding of individual axial fibers from the matrix. Progressive debonding is probably the only significant damage sustained by the composite up to 60 percent of its fatigue life.

2. At 60 percent of life, debonding has occurred to a degree sufficient to permit local buckling of individual fibers or groups

of adjacent fibers. This accelerated damage rate appears as an increase in the permanent strain accumulation rate during the last 40 percent of life.

3. Fatigue life may be predicted either from a linear relationship on the S-logN diagram, or from a measurement of life to the point at which the strain accumulation rate changes.

4. Slight misalignment of a small percentage of the axial plies or sea water immersion causes only a small reduction in fatigue strength.

APPENDIX A

Manufacturer's Technical Data

General Description

Material Designation	Type 1002 Scotchply
Temperature Range in Service	-60°F to 250°F
Average Uncured Thickness (in.)	0.011
Resin Content, Uncured (%)	36% by weight
Type of Matrix	Epoxy

Physical Properties, Cured Laminate

Flammability (in/min)	0.10
Barcol Hardness	70
Rockwell Hardness (M Scale)	100 - 108
Specific Gravity	1.84
Molded thickness, one ply (in)	0.010
Wet Strength Retention (%, 2 hr. boil)	86

Mechanical Properties (Stress Angle 0°, Temperature 70°F)

	Unidirectional Laminate	Crossplied Laminate
Flexure Strength (psi x 10^3)	165	120
Modulus in Flexure (psi x 10^6)	5.3	3.5
Tensile Strength (psi x 10^3)	160	75
Modulus in Tension (psi x 10^6)	5.7	3.7
Compressive Strength, Edge (psi x 10^3)	90	75
Izod Impact, Edge (ft. lb./in. notch)	60.8	35.2
Interlaminar Shear Strength (psi x 10^3)	4.3	4.1

Chemical Properties

Water Absorption, 24 hour immersion (%)	0.05
Water Absorption, 7 day immersion at 70°F:	
Change in Weight (%)	+0.17
Change in Thickness (%)	+0.09
Flexural Strength (psi x 10^3)	109
Specific Heat (cal/gm-°C)	0.21

TABLE 1

FABRICATION DATA SUMMARY

Laminate	Plies	Length x Width	Configuration	Releasing Agent
6	30	12" x 12"	Standard[a]	S.C.W. 33 Silicon Paper
9-15	30	6" x 6"	Standard with 4 plies misaligned at 15°[b]	S.C.W. 33 Silicon Paper
9-30	30	6" x 6"	Standard with 4 plies misaligned at 30°[b]	S.C.W. 33 Silicon Paper
9-45	30	6" x 6"	Standard with 4 plies misaligned at 45°	S.C.W. 33 Silicon Paper
10	30	12" x 12"	Standard	S.C.W. 33 Silicon Paper
11	30	12" x 12"	Standard	"Frekote" on Mylar
12-30	36	8" x 12"	Standard with 4 plies misaligned at 30°[c]	"Frekote" on Mylar
13-15	36	8" x 12"	Standard with 4 plies misaligned at 15°[c]	"Frekote" on Mylar

a Standard configuration is defined as alternating plies of 0° and 90°.

b The misaligned plies were not at the laminate center due to a fabrication error.

c The misaligned plies were located at center of the laminate.

Laminate Number	6	9-15	9-30	9-45	10	11* 11(SW)	12-30	13-15
Ultimate Compressive Strength (psi)	70,300	64,900	47,300	49,800	83,200	89,000 (77,800)	53,200	75,800
Range of Cyclic Test (Maximum Cycles)	600	200	150	150	167	120 (114)	250	205
γ_V (Vol. %) Burnout Method	6.55	4.4	4.27	7.0	2.40	2.25 (2.60)	2.0	4.25
γ_V (Vol. %) Point Count Method	8.50	--	--	--	5.33	4.67 (6.15)	--	--
γ_R Vol. %	47.6	37.6	33.3	33.7	39.0	36.6 (34.6)	33.0	35.4
γ_G Vol. %	45.9	58.0	62.4	59.3	58.6	61.1 (60.7)	65.0	60.3
Post-Cured Specific Gravity ρ_c	1.79	1.96	2.03	1.98	2.01	2.05 (2.03)	2.10	2.02

*Data in parentheses measured after sea water immersion.

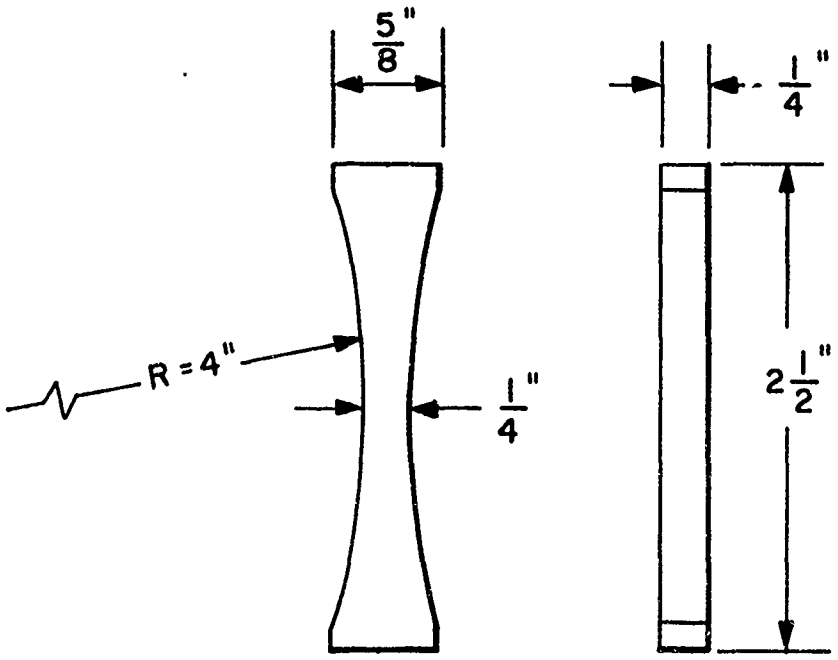

Figure I. Fatigue Specimen Geometry

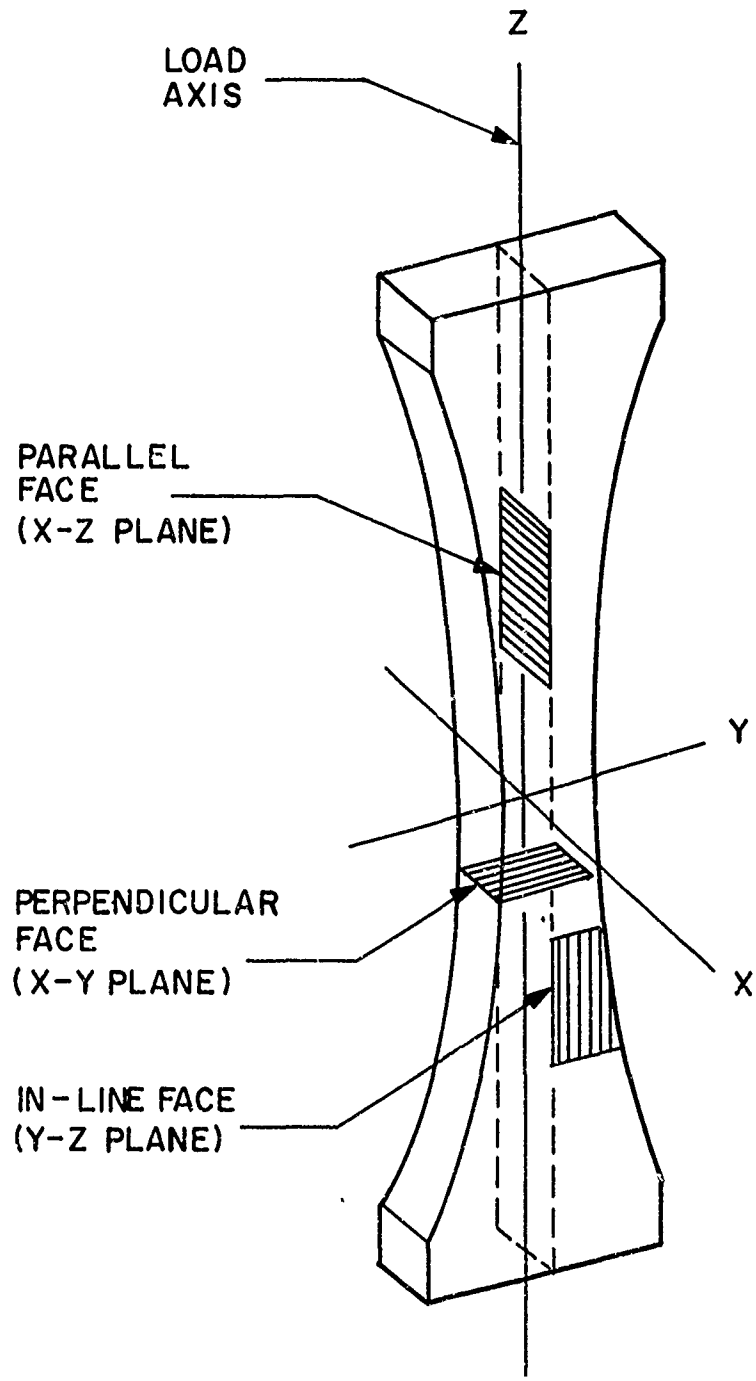

Figure 2. Orientation of Sections for Microscopic Analysis

Figure 3a

Figure 3b

Figure 3c

Typical Failures

Figure 3

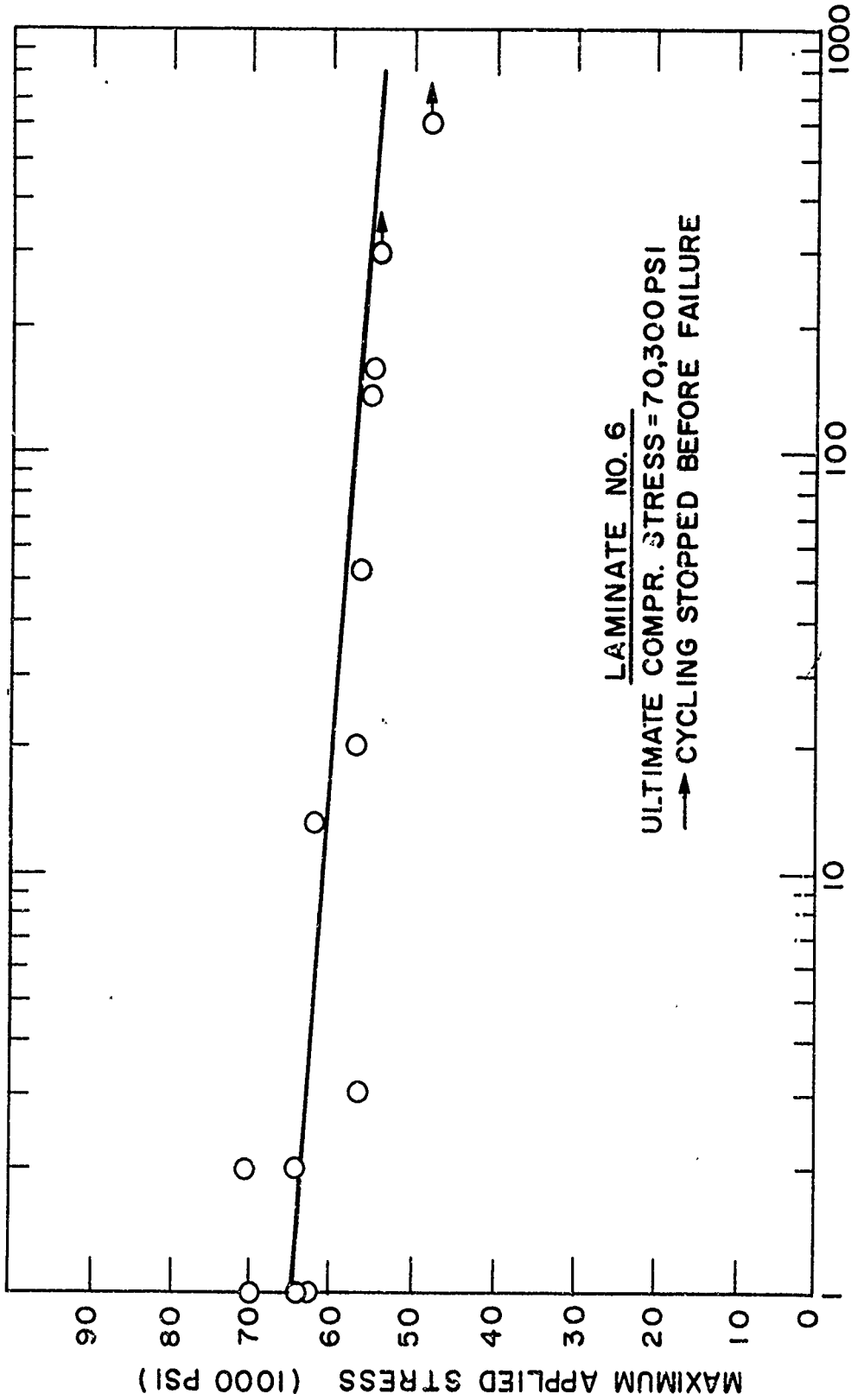

Figure 4 S-N Curve for Compressive Fatigue Test of Laminate 6

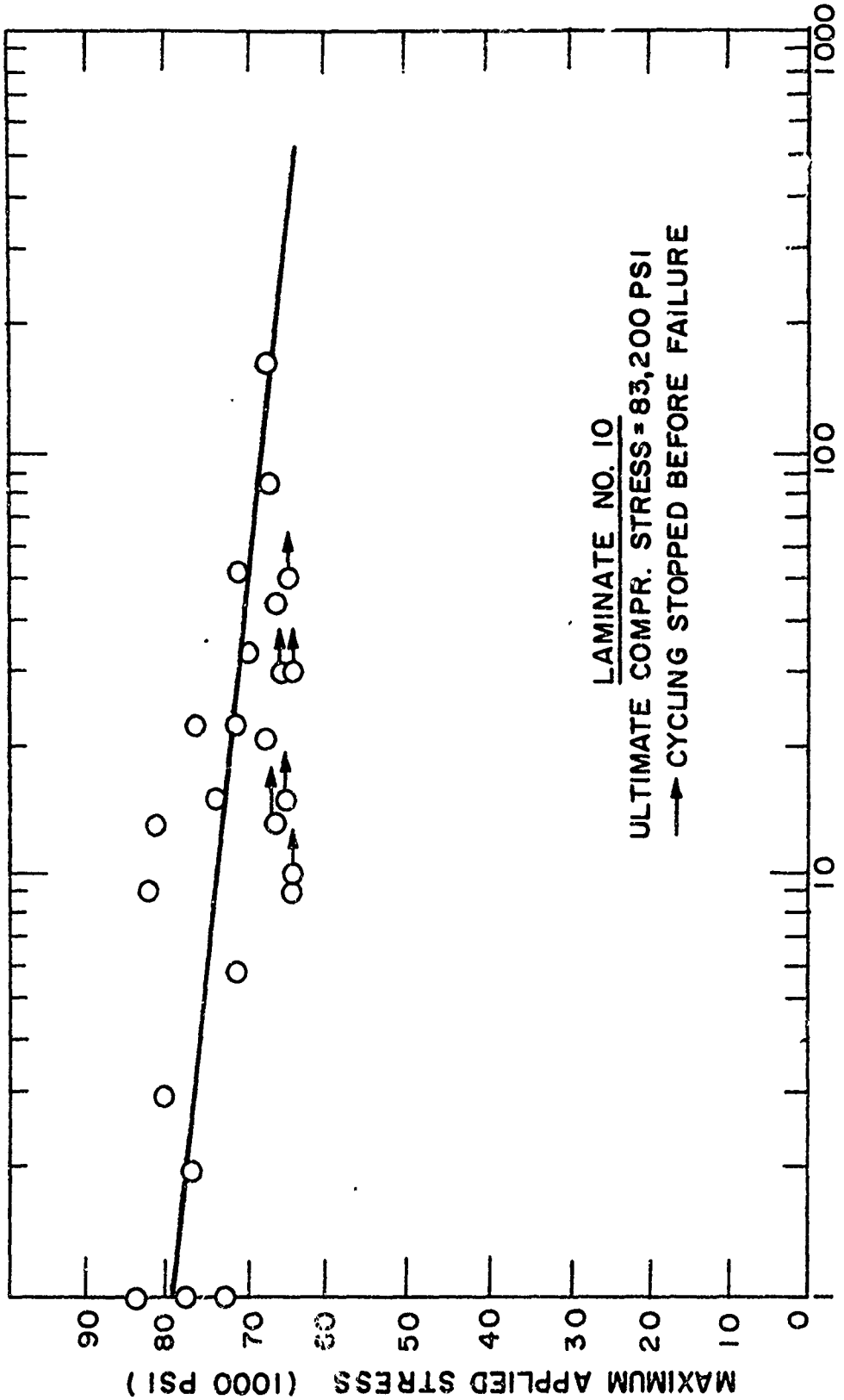

Figure 5. S-N Curve for Compressive Fatigue Test of Laminate 10

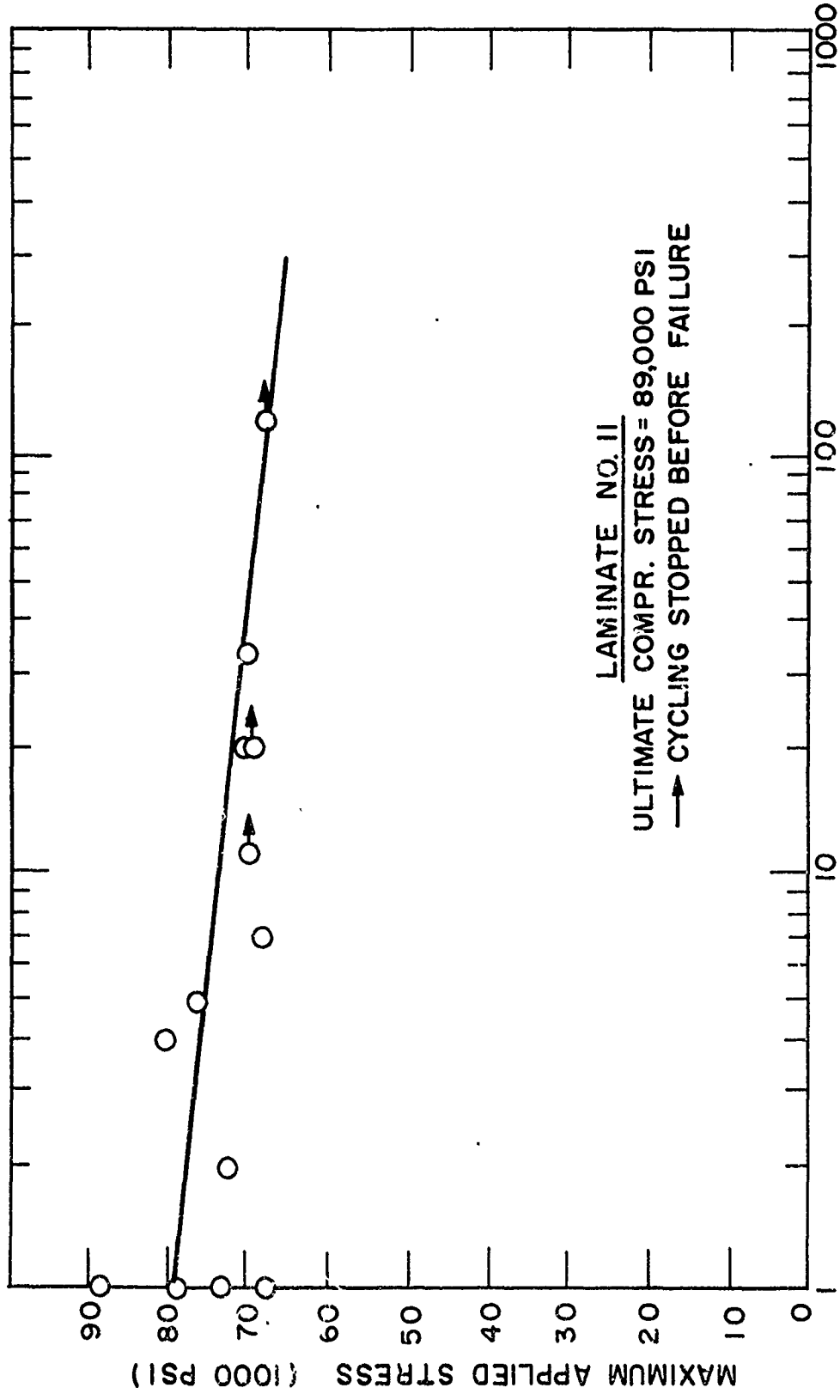

Figure 6. S-N Curve for Compressive Fatigue Test of Laminate II.

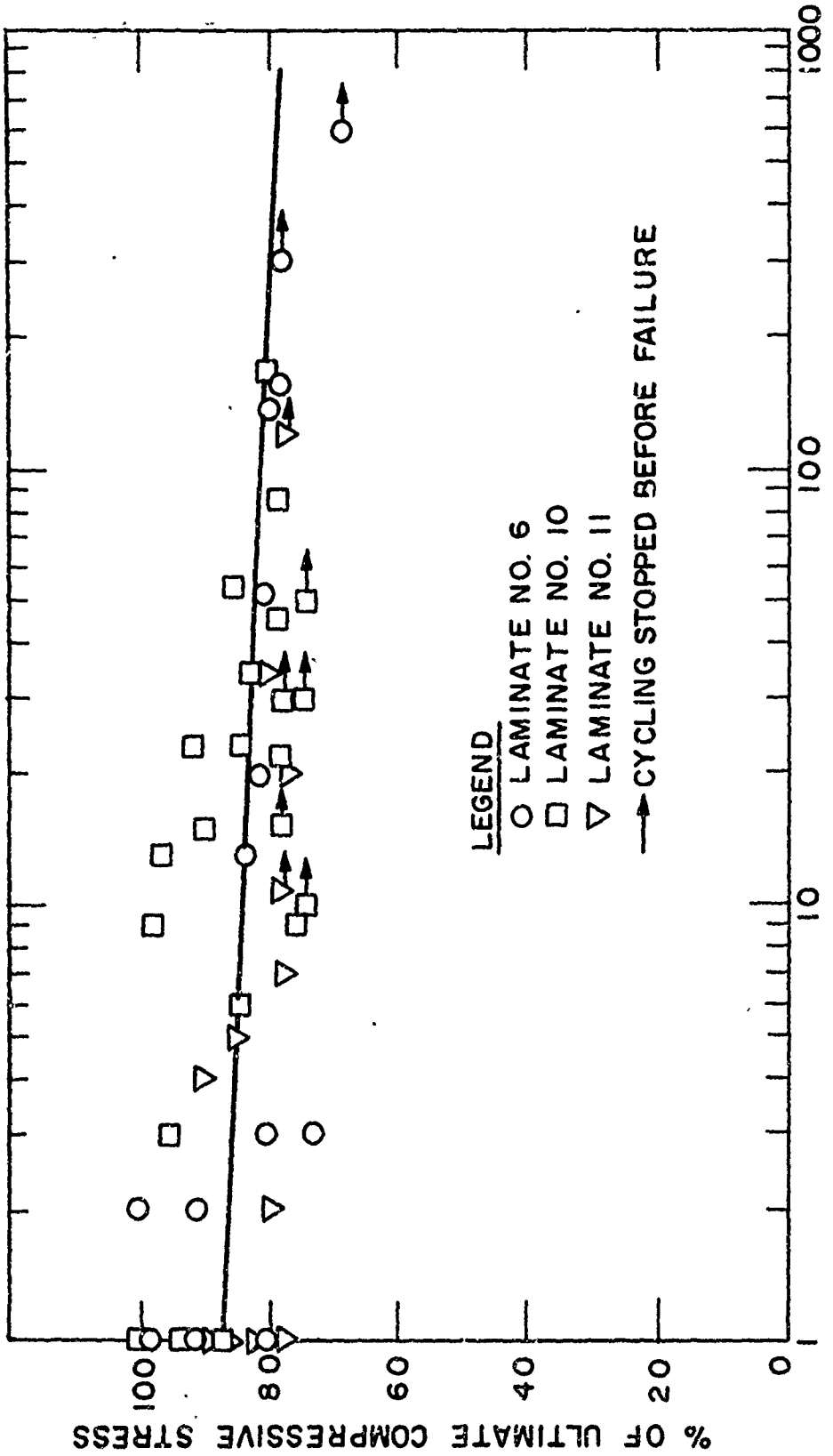

Figure 7. Combined S-N Curve for Compressive Fatigue Tests of Laminates 6, 10, and 11.

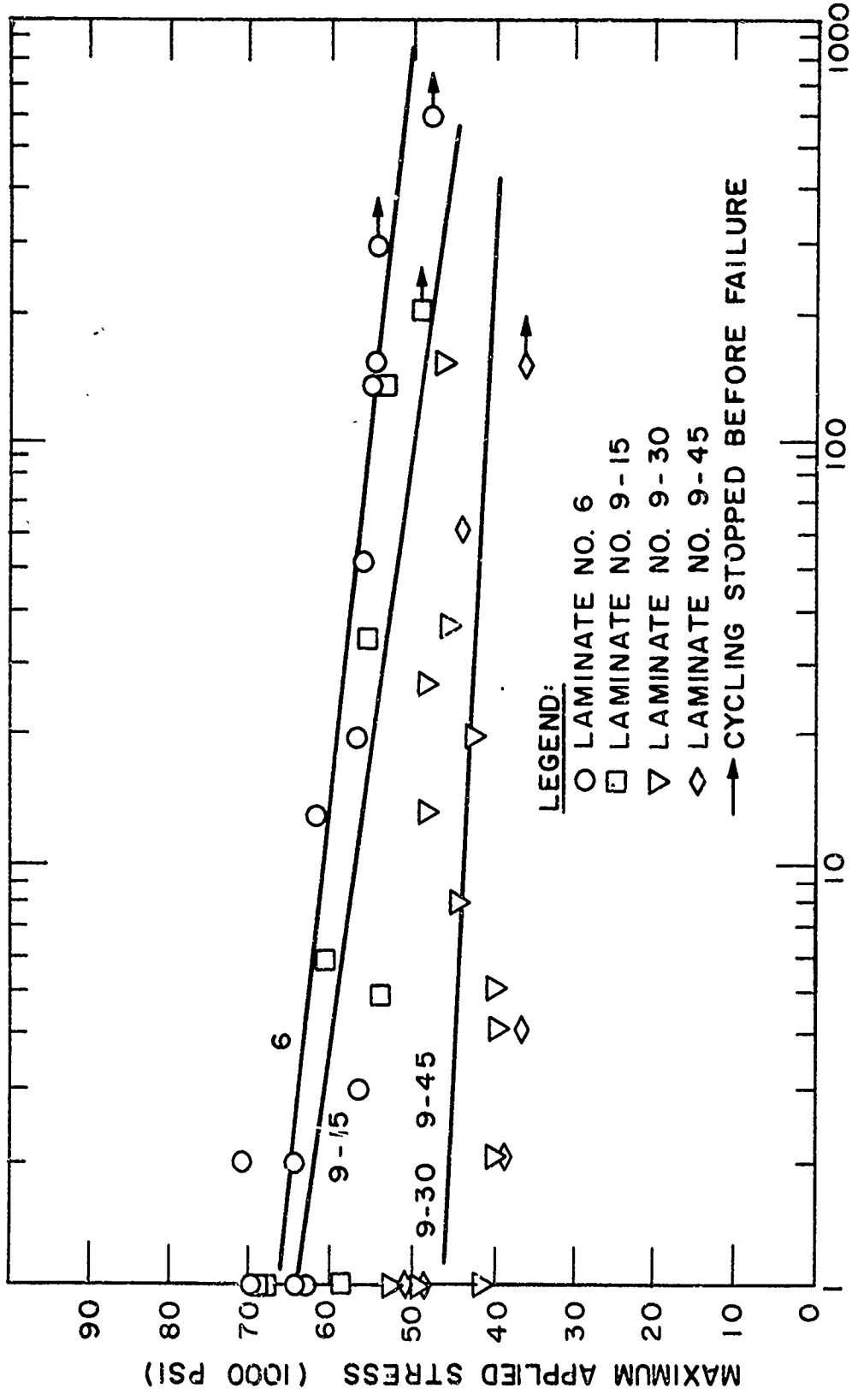

Figure 8. S-N Curves for Compressive Fatigue Tests of Misaligned Laminate 9. Laminate 6 Data Included for Reference

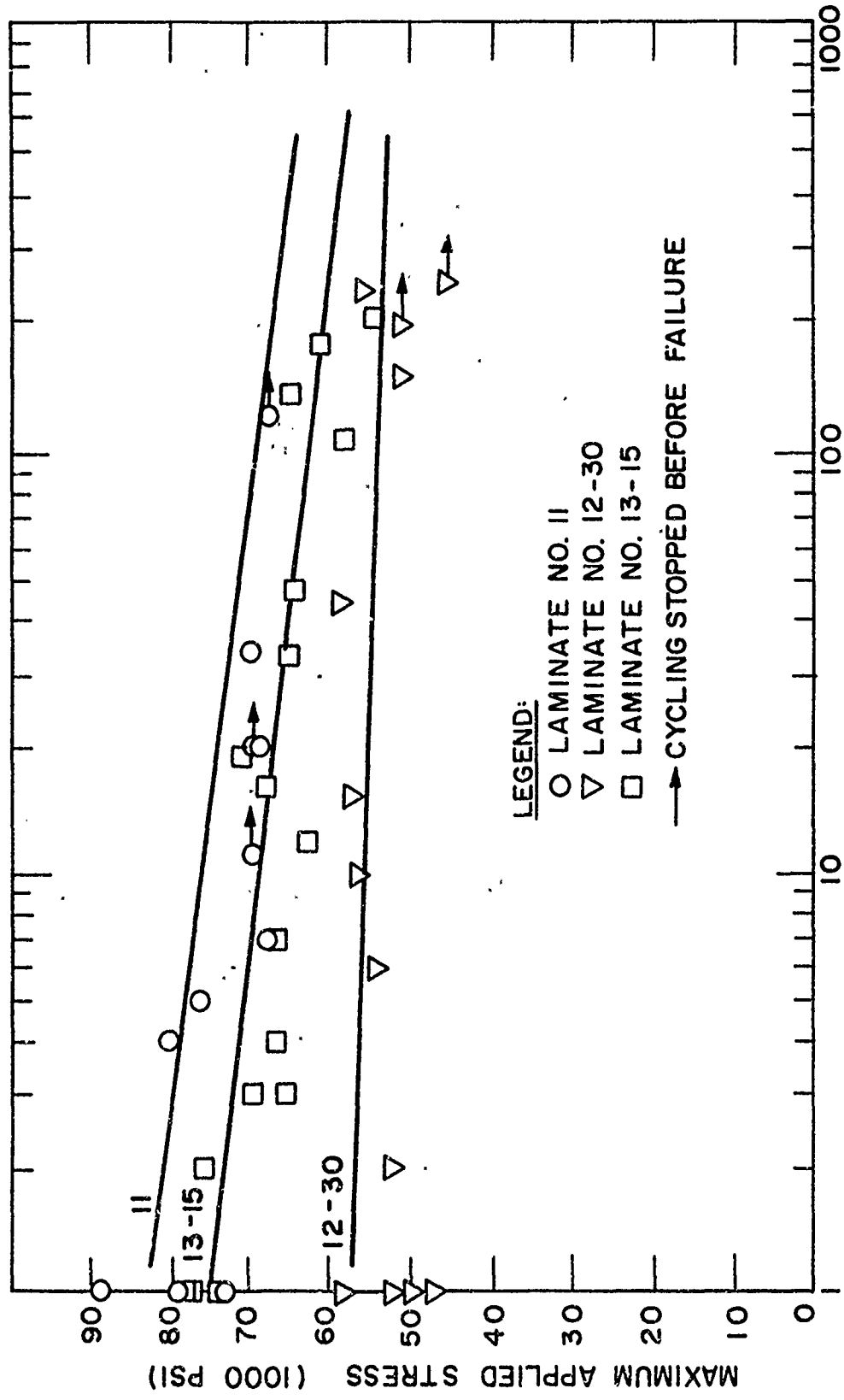

Figure 9. S-N Curves for Compressive Fatigue Tests of Misaligned Laminates 12 and 13. Laminate 11 Data included for Reference

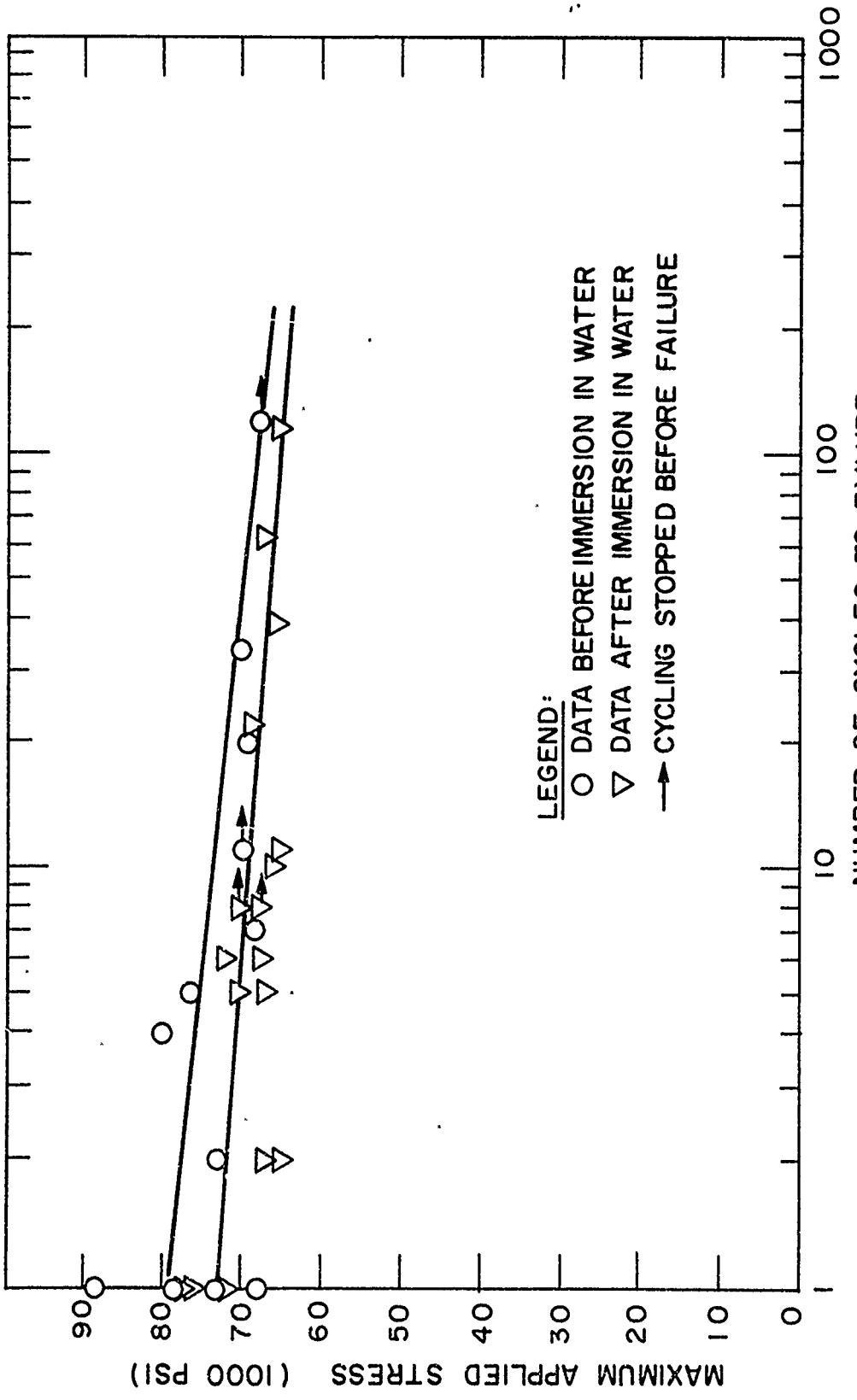

Figure 10. S-N Curves for Compressive Fatigue Tests of Laminate II, showing effects of Sea Water Immersion

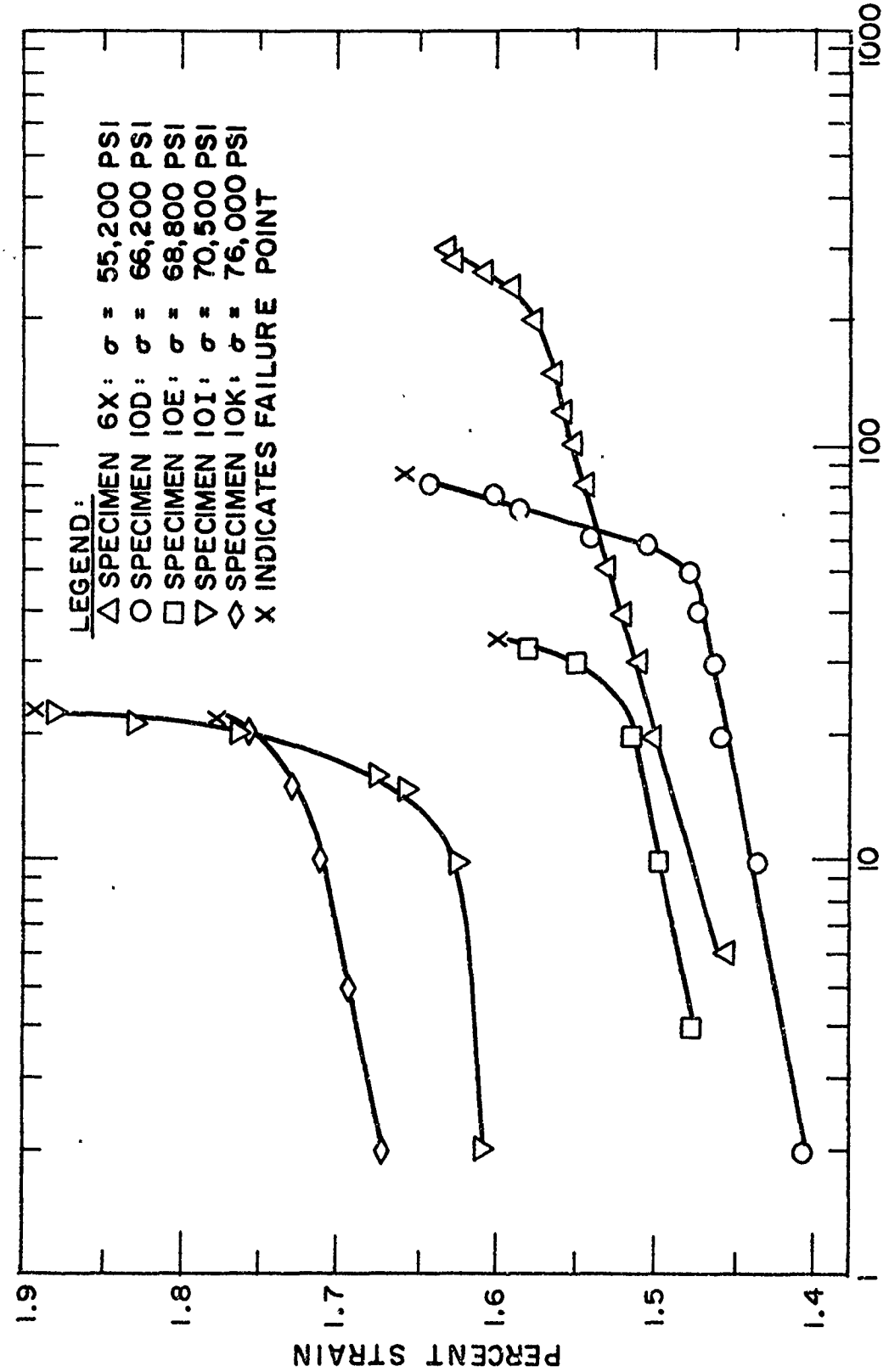

Figure 11. Strain History of Selected Specimens During Compressive Fatigue Testing, Showing Sudden Increase in Strain Accumulation Rate at Approximately 60% of Fatigue Life

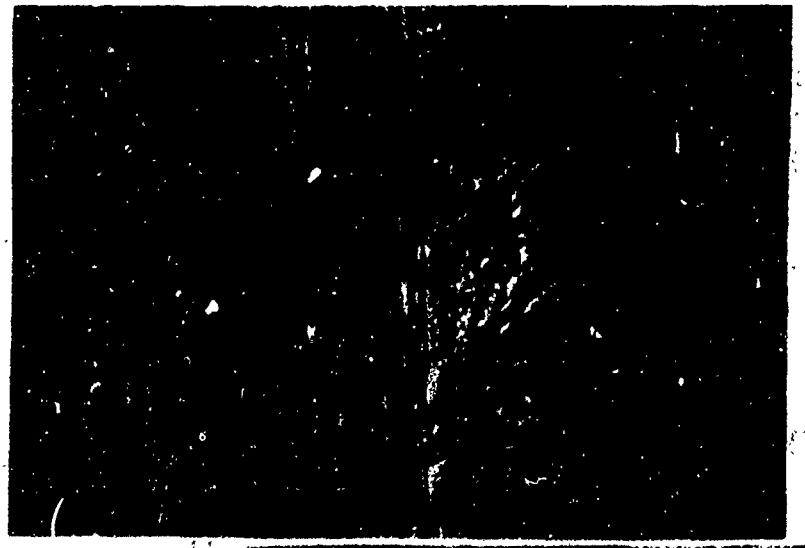

Figure 12

Laminate #11
Reference
120X
Parallel Face

Figure 13

#11 BE
69,400 psi
20 Cycles
No Failure
120X
Parallel Face
Load Direction
is Vertical

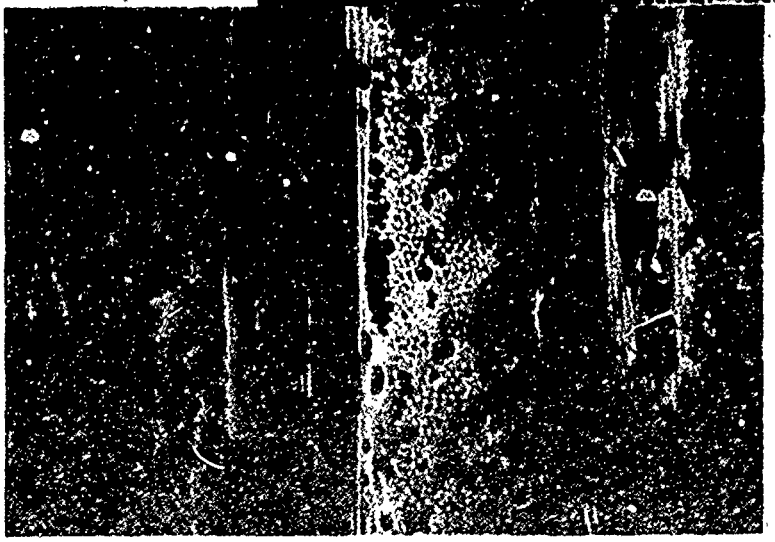

Figure 14

#11W
68,000 psi
120 Cycles
No Failure
120X
Parallel Face
Load Direction
is Vertical

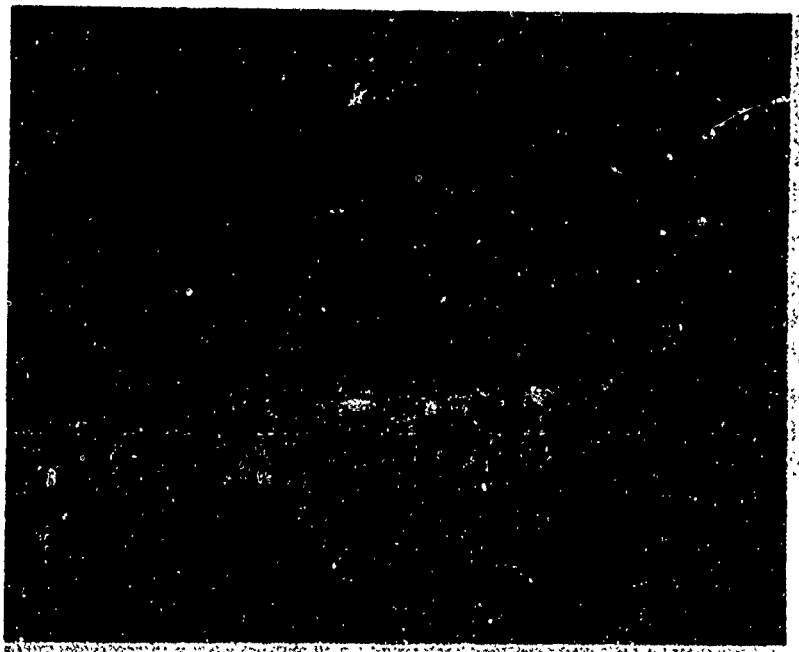

Figure 15

#11W

68,000 psi

120 Cycles

No Failure

120X

Perpendicular Face

Load Direction is

Out of the Page

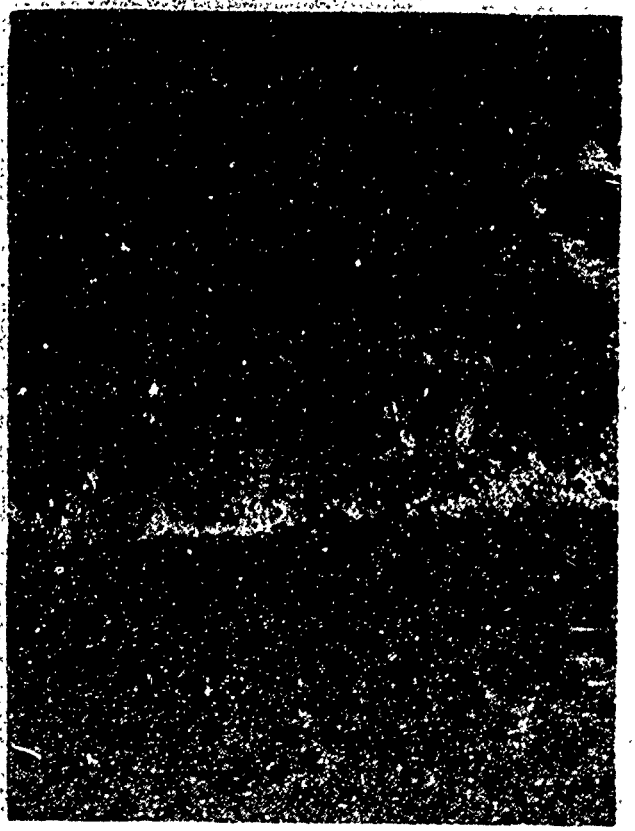

Figure 16

#11BD

61,000 psi

½ Cycle

Failure

120X

Perpendicular Face

Load Direction is

Out of the Page

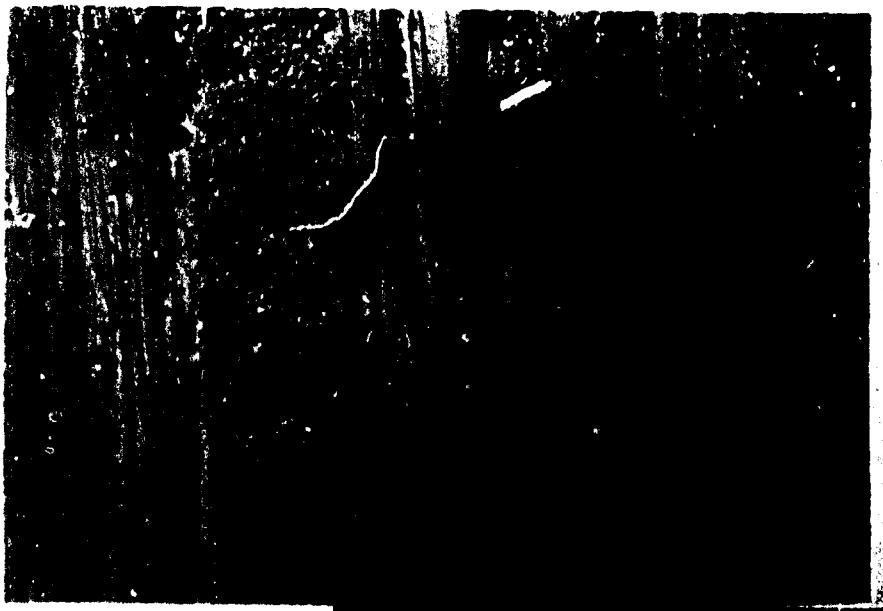

Figure 17
Laminate #10
Reference
120X
Parallel Face

Figure 18
#10U
69,400 psi
30 Cycles
No Failure
120X
Parallel Face
Load Direction
is Vertical

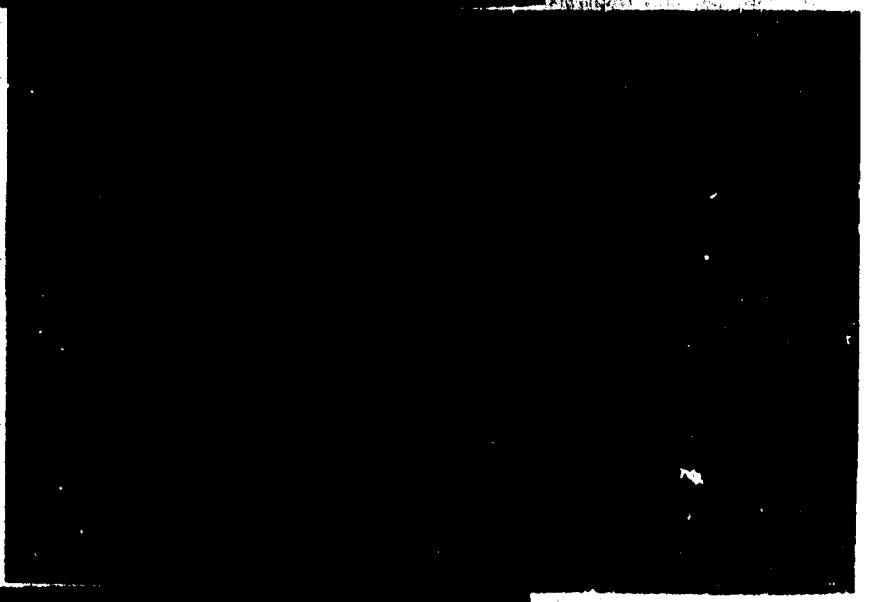

Figure 19
#10N
81,000 psi
13 Cycles
Failure
120X
Perpendicular Face
Load Direction is
Out of the Page

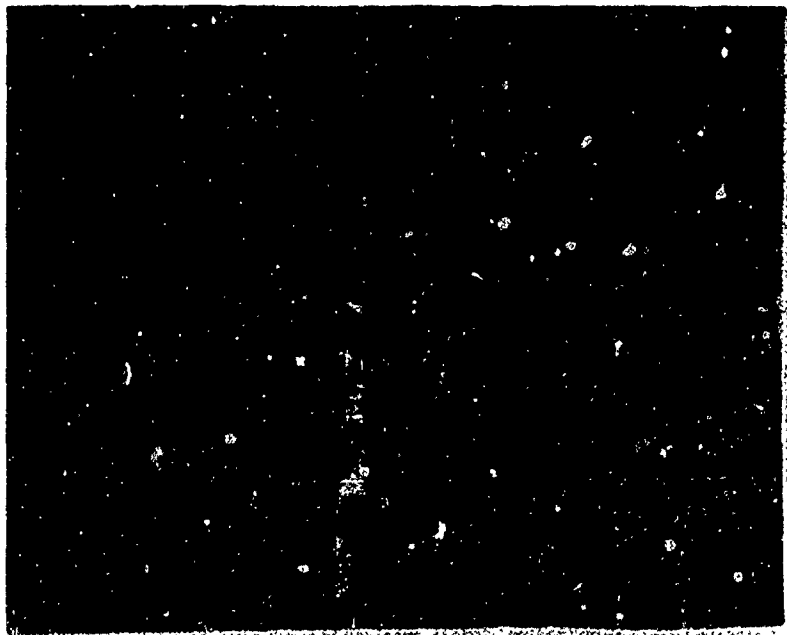

Figure 20
Laminate #6
Reference
120X
Parallel Face

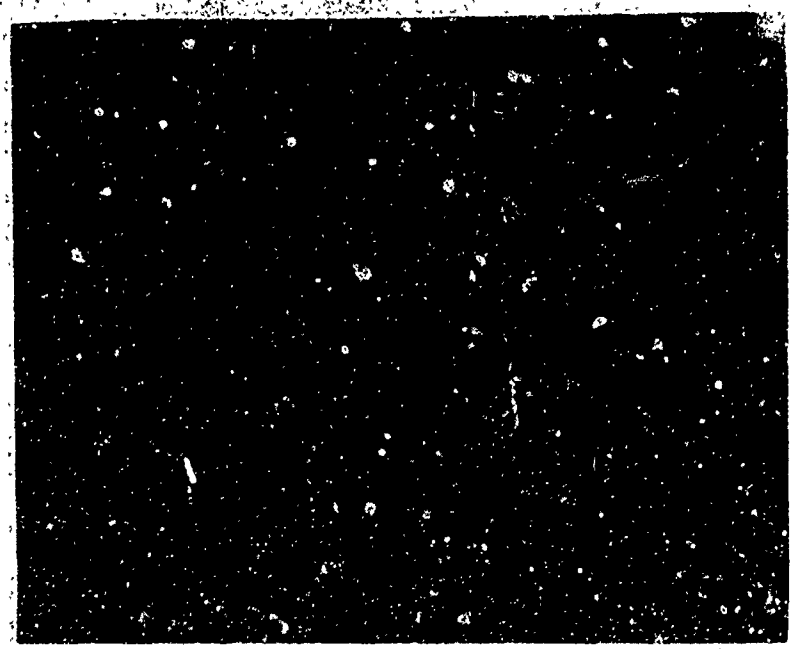

Figure 21
#11BK
70,000 psi
11 Cycles
No Failure
120X
Parallel Face
Load Direction
is Vertical

Figure 22
#11AC
67,500 psi
½ Cycle
Surface Crack
In Line Face
120X
Load Direction is
Vertical

Figure 23
#11BD
61,000 psi
½ Cycle
Failure
120X
Surface Crack
Parallel Face
Load Direction
is Vertical

Figure 24 12-30-I, 52,400 psi, 2 cycles, failure, 120X, parallel face, load direction is vertical, misaligned fibers on left.

Figure 25 12-30-J, 54,600 psi, 6 cycles, failure, 120X, parallel face, load direction is vertical, misaligned fibers on left.

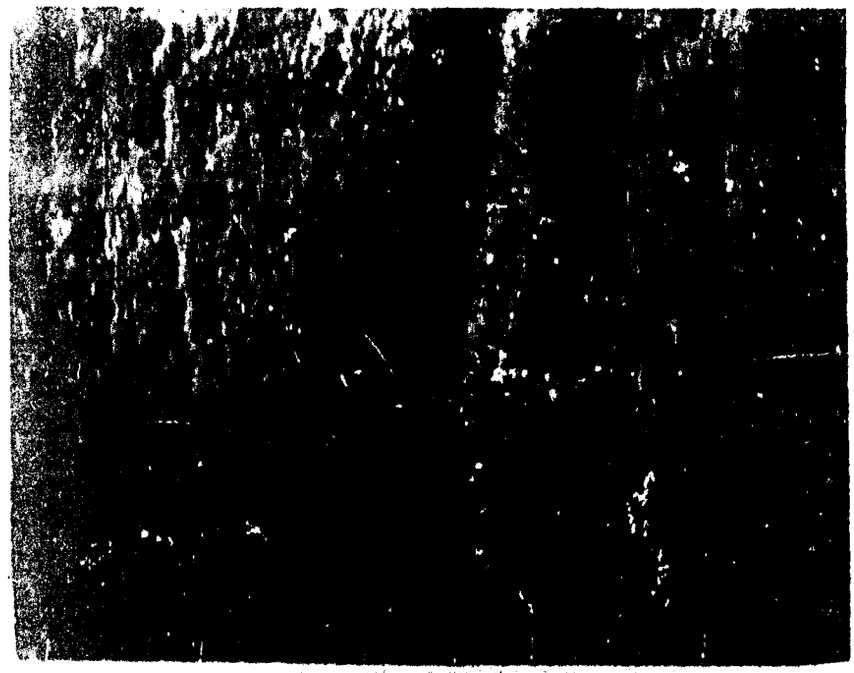

Figure 26 12-30-I, 52,100 psi, 2 cycles, failure, 120X, perpendicular face, load direction is out of the page. Misaligned fibers on left.

Figure 27 9-45-E, 38,300 psi, 4 cycles, failure, 120X, face shown is 45° plane through center of specimen, broken fibers are 45° misaligned fibers, fiber ends on left are vertical fibers in line with the load.

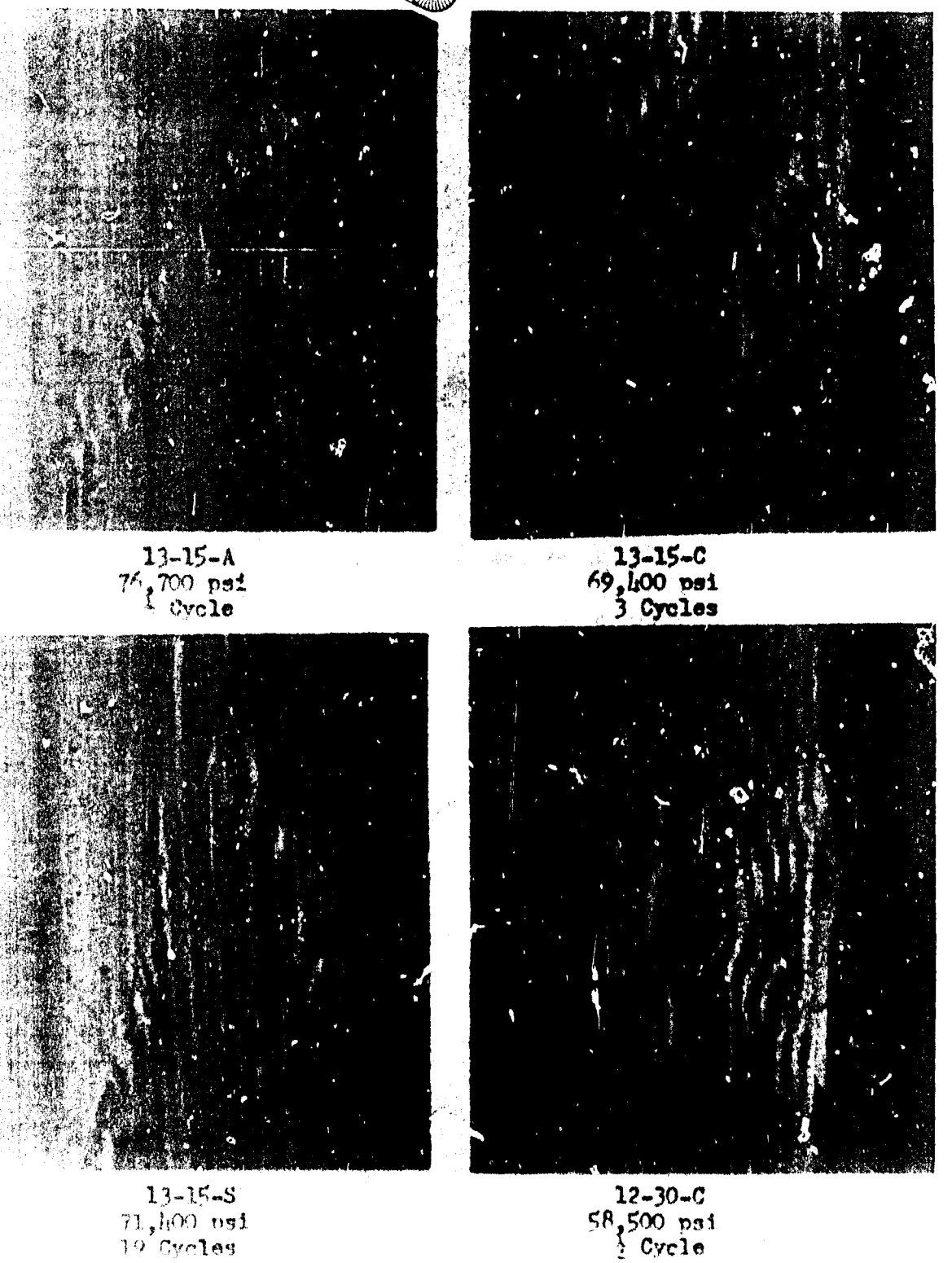

13-15-A
76,700 psi
1 Cycle

13-15-C
69,400 psi
3 Cycles

13-15-S
71,400 psi
12 Cycles

12-30-C
58,500 psi
½ Cycle

Fig. 28 Typical Failures of Specimens with Misaligned Fibers at the Center of the Cross Section. 7X

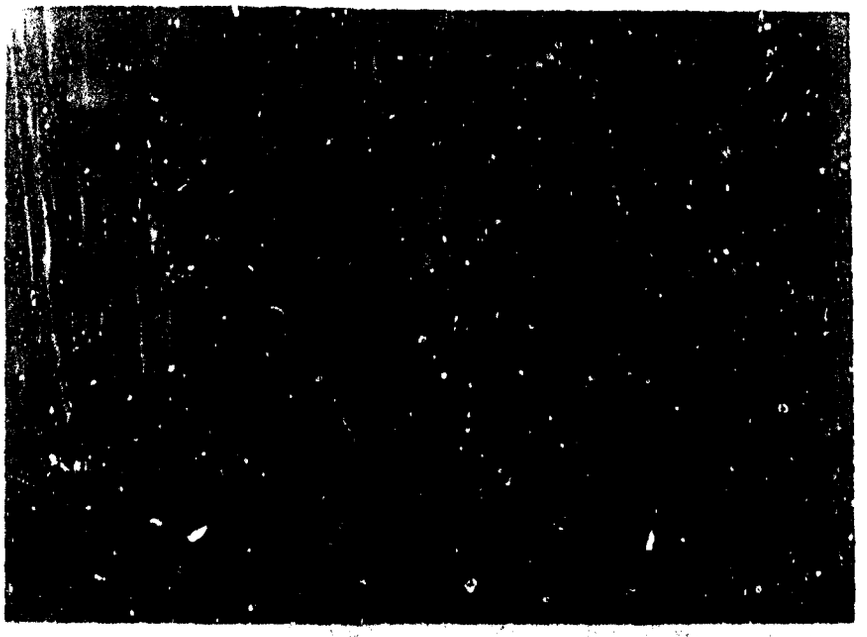

(a)

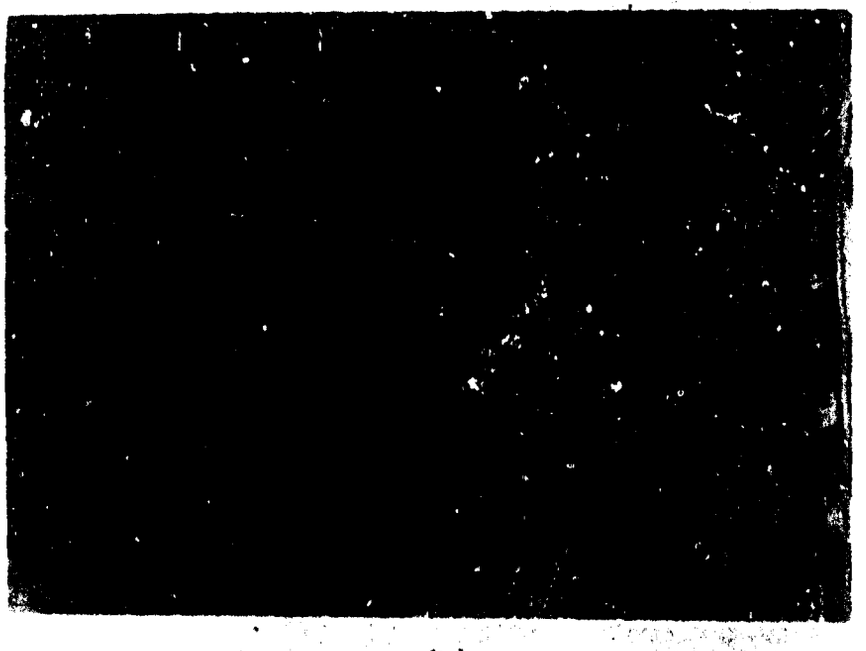

(b)

Figure 29 Specimen Number 11V (SW), Parallel Face, 120X. Reference Specimen, No Load Applied. Shown After Sea Water Immersion.

(a) Perpendicular face, showing damage in layer with fibers perpendicular to axis of load. Load applied perpendicular to plane of paper.

(b) Parallel face, showing damage in layer with fibers parallel to axis of load. Load applied in vertical direction.

30 Specimen 11H (3/4", 13%, Fatigue Tested for 8 Cycles at 70,000 psi after 24 Hour Water Immersion. Cycling Stopped Before Failure.

(a) Perpendicular face, showing interlaminar separation. Load applied perpendicular to plane of paper.

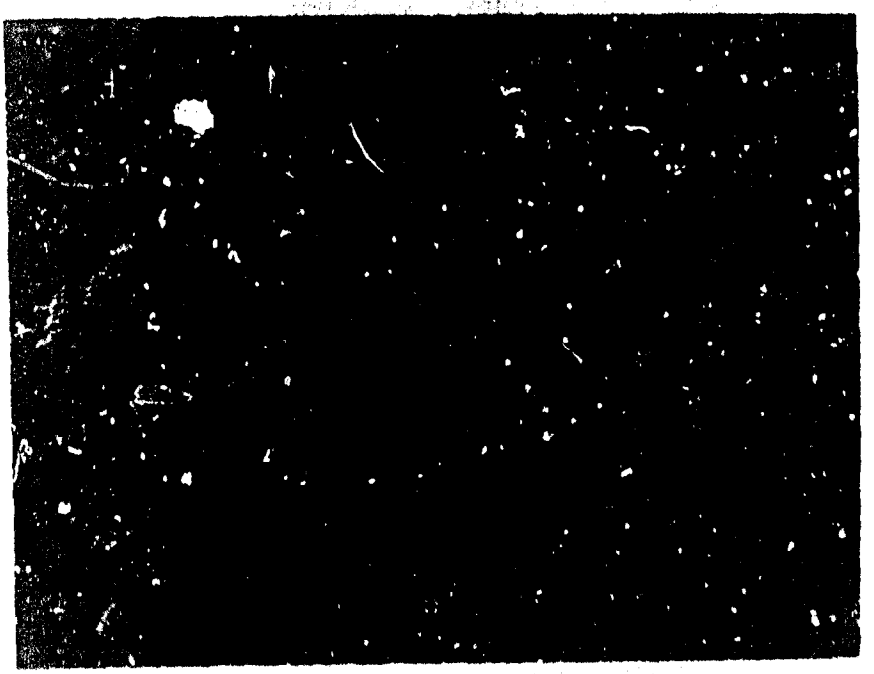

(b) Parallel face, showing damage in layer with fibers perpendicular to axis of load. Load applied in vertical direction.

Figure 31 Specimen 11P (SW), 120X, Fatigue Tested to Failure After Sea Water Immersion. Failure After 10 Cycles at 66,500 psi.

REFERENCES

1. ASTM Designation D695-68T, "Tentative Method of Test for Compressive Properties of Rigid Plastics," ASTM, Phila., Pa.
2. Boller, K. H., "Effect of Pre-Cyclic Stresses on Fatigue Life of Plastic Laminates Reinforced with Unwoven Fibers," AFML-TR-64-168, Air Force Materials Laboratory, Wright-Patterson AFB, Ohio, September 1964.
3. Boller, K. H., "Fatigue Strength of Plastic Laminates Reinforced with S Glass Fibers," AFML-TR-64-403, Air Force Materials Laboratory, Wright-Patterson AFB, Ohio, May 1965.
4. Boller, K. H., "Fatigue Characteristics of Two New Plastic Laminates Reinforced with Unwoven S Glass Fibers, Under Cyclic Axial and Shear Loading," AFML-TR-66-54, Air Force Materials Laboratory, Wright-Patterson AFB, Ohio, May 1966.
5. Boller, K. H., "Effect of Single-Step Change in Stress on Fatigue Life of Plastic Laminates Reinforced with Unwoven E Glass Fibers," AFML-TR-66-220, Air Force Materials Laboratory, Wright-Patterson AFB, Ohio, December 1966.
6. Boller, K. H. and Stevens, G. H., "Effect of Type of Reinforcement on Fatigue Properties of Plastic Laminates," A.S.T.I.A. Document No. 213835, Wright Air Development Center, Ohio, May 1959.
7. Broutman, L. J. and Krock, R. H. (editors), Modern Composite Materials, Addison-Wesley, 1967.
8. Broutman, L. J. and Sahu, S., "Progressive Damage of a Glass Reinforced Plastic During Fatigue," Proc. 20th Annual Conf., Reinf. Plastics Div., SPI, Section 11-D, 1969.
9. Broutman, L. J., "Failure Mechanisms for Filament Reinforced Plastics," Modern Plastics, April 1965.
10. Cole, C. K., Cornish, R. H. and Elliott, J. P., "Effect of Voids and Structural Defects on the Compressive Fatigue of Glass Reinforced Plastics," Proc. 21st Annual Conf., Reinf. Plastics Div., SPI, Section 17-C, 1966.

11. DeHoff, R. T. and Rhines, F. N., Quantitative Microscopy, McGraw-Hill, 1968.
12. Freund, J. F. and Silvergleit, M., "Fatigue Characteristics of Glass Reinforced Plastic Material," Proc. 21st Annual Conf., Reinf. Plastics Div., SPI, Section 17-B, 1966.
13. Fried, N., "The Response of Orthogonal Filament Wound Materials to Compressive Stress," Proc. 20th Annual Conf., Reinf. Plastics Div., SPI, Section 1-C, 1965.
14. Fried, N., Kaminetsky, J. and Silvergleit, M., "Development of Filament Wound Plastics with Enhanced Compressive Properties through Use of Improved Resin Systems," Proc. 22nd Annual Conf., Reinf. Plastics Div., SPI, Section 20-B, 1967.
15. Graner, W. R., "Reinforced Plastics for Deep-Submergence Application," Ocean Engineering, Vol. 1, 1969.
16. Hilliard, J. E. and Cahn, J. W., "An Evaluation of Procedures in Quantitative Metallography for Volume-Fraction Analysis," Trans. Met. Soc. AIME, Vol. 221, 1961, pp. 344-352.
17. Hom, K., "Composite Materials for Pressure Hull Structures," U. S. Naval Applied Science Laboratory - Polytechnic Institute of Brooklyn Symposium, Materials - Key to Effective Use of the Sea, September 12-14, 1967.
18. Hom, K., Buhl, J. E. and Willner, A. R., "Glass Reinforced Plastics for Submersible Pressure Hulls," Naval Eng. J., Vol. 75, No. 4, October 1963.
19. Hom, K. et. al., "Investigation of Filament Reinforced Plastics for Deep-Submergence Application," AD 645 960, David Taylor Model Basin, Washington, D. C., November 1966.
20. 3M Company Memorandum, "3M Scotchply Pre-impregnated Glass Fiber Molding Materials," 3M Co., St. Paul, Minn., January 1963.
21. 3M Company Memorandum, "Scotchply Type 1002 Resin Casting Tested per ASTM Procedure at 73°F," 3M Co., St. Paul, Minn.

22. Myers, N. and Fink, B., "Filament Wound Structural Model Studies for Deep Submergence Vehicles," Naval Eng. J., Vol. 77, No. 2, April 1965.
23. Otto, W. H., "Compaction Effects in Glass Fibers," Amer. Ceramic Soc. J., Vol. 44, No. 2, February 1961, pp. 68-72.
24. Rosen, B. W., "Mechanics of Composite Strengthening," Fiber Composite Materials, Amer. Soc. for Metals, 1964.
25. Sedor, G., "An Investigation into the Low Cycle Compressive Fatigue Failure Mechanism of a Composite Material," SM Thesis, Dept. of Ocean Engineering, M.I.T., June 1970.
26. Watterson, R. K., "High Compressive Stress, Low Cycle Fatigue of a Composite Material," SM Thesis, Dept. of Ocean Engineering, M.I.T., May 1970.